HHS Public Access

Author manuscript

Nat Cell Biol. Author manuscript; available in PMC 2020 September 30.

Published in final edited form as:

Nat Cell Biol. 2020 April ; 22(4): 372–379. doi:10.1038/s41556-020-0493-0.

RNA helicase DDX21 mediates nucleotide stress responses in neural crest and melanoma cells

Cristina Santoriello[#1,2], **Audrey Sporrij**[#1,2], **Song Yang**[1,2], **Ryan A. Flynn**[3], **Telmo Henriques**[4], **Bilguujin Dorjsuren**[1,2], **Eugenia Custo Greig**[1,2], **Wyatt McCall**[1,2], **Meredith E. Stanhope**[1,2], **Maurizio Fazio**[1,2], **Michael Superdock**[1,2], **Asher Lichtig**[1,2], **Isaac Adatto**[1], **Brian J. Abraham**[5], **Marian Kalocsay**[6], **Michael Jurynec**[7], **Yi Zhou**[1,2], **Karen Adelman**[4], **Eliezer Calo**[8], **Leonard I. Zon**[1,2,*]

[1]Department of Stem Cell and Regenerative Biology, Harvard University, Cambridge, MA 02138, USA

[2]Stem Cell Program and Division of Hematology/Oncology, Boston Children's Hospital, Harvard Stem Cell Institute, Howard Hughes Medical Institute, Harvard Medical School Boston, MA 02115, USA

[3]Department of Chemistry, Stanford University, Stanford, California 94305, USA

[4]Department of Biological Chemistry and Molecular Pharmacology, Harvard Medical School, Boston, MA 02115, USA

[5]Whitehead Institute for Biomedical Research, MIT, Cambridge, MA 02142, USA

[6]Laboratory of Systems Pharmacology, Harvard Medical School, Boston, MA, 02115 USA

[7]University of Utah Department of Orthopedics, Salt Lake City, UT 84108, USA

[8]Department of Biology and Koch Institute for Integrative Cancer Research, Massachusetts Institute of Technology, Cambridge, MA 02142, USA

[#] These authors contributed equally to this work.

Abstract

The availability of nucleotides has a direct impact on transcription. Inhibition of dihydroorate dehydrogenase (DHODH) with leflunomide impacts nucleotide pools by reducing pyrimidine levels. Leflunomide abrogates effective transcription elongation of genes required for neural crest development and melanoma growth *in vivo*[1]. To define the mechanism of action, we undertook an

[*]Correspondence to: leonard.zon@enders.tch.harvard.edu.

Author Contributions

C.S. designed the study. C.S., A.S, B.D., W.M., E.C.G., M.E.S., M.F., performed experiments. A.L., M.S., B.J.A., S.Y., provided formal data analysis. I.A. assisted with the zebrafish logistics. T.H., R.A.F., M.K., E.C., performed experiments and analysed data. M.J, K.A., T.H., and Y.Z., provided insights on data interpretation. C.S., A.S., and L.I.Z. wrote the manuscript. L.I.Z. conceived and managed the study.

Conflict of Interests

B.J.A. is a shareholder of Syros Pharmaceuticals. L.I.Z. is founder and stockholder of Fate, Inc., Scholar Rock, Camp4 therapeutics and a scientific advisor for Stemgent. The other authors declare no competing interests.

in vivo chemical suppressor screen for restoration of neural crest after leflunomide treatment. Surprisingly, we found that alterations in progesterone and progesterone receptor (Pgr) signalling strongly suppressed leflunomide-mediated neural crest effects in zebrafish. Progesterone additionally bypasses the transcriptional elongation block resulting from Paf complex deficiency, rescuing neural crest defects in *ctr9* morphant and *paf1(aln^{z24})* mutant embryos. Using proteomics, we found that Pgr binds the RNA helicase protein Ddx21. *Ddx21*-deficient zebrafish show resistance to leflunomide-induced stress. On a molecular level, nucleotide depletion reduced the chromatin occupancy of DDX21 in human A375 melanoma cells. Nucleotide supplementation reversed the gene expression and DDX21 occupancy changes prompted by leflunomide. Together, our results show that DDX21 acts as a sensor and mediator of transcription during nucleotide stress.

Maintenance of adequate nucleotide pools is necessary for many biological processes[2]. Changes in nucleotide metabolism can cause cellular transformation and tumorigenesis[3,4]. Inhibition of DHODH, an enzyme involved in *de novo* nucleotide biosynthesis, lowers pyrimidine levels and blocks transcription elongation in neural crest and melanoma[1]. Transcription elongation is highly regulated following recruitment of RNA polymerase II (Pol II) to the transcriptional start site (TSS) and establishment of promoter-proximal pausing[5,6]. The positive transcription elongation factor b (p-TEFb), composed of cyclin-dependent kinase 9 (CDK9) and cyclin T1 (CCNT1), is able to relieve pausing and stimulate productive elongation[7,8]. HEXIM1, a component of the 7SK small nuclear ribonuclear protein (7SK snRNP), sequesters p-TEFb to enforce transcriptional pausing under nucleotide stress[9]. Despite these insights, the mechanisms through which nucleotide depletion is sensed are unknown.

To elucidate how a block in pyrimidine biosynthesis affects transcription elongation, we performed a chemical suppressor screen for the DHODH inhibitor leflunomide in zebrafish (*Danio rerio*). We treated embryos with leflunomide and screened 2140 chemicals by *whole mount in situ hybridization* (*WISH*) for the neural crest marker *crestin*[10] (Fig. 1a). We identified 30 compounds that were able to rescue the neural crest lineage upon leflunomide treatment (Supplementary Table 1). To ensure specificity, we tested these chemicals in combination with A77 1726 (Terileflunomide), the active metabolite of leflunomide, and 2-[(3,5-Difluoro-3'-methoxy-4-biphenylyl)amino]nicotinic acid, a DHODH inhibitor with a distinct chemical structure hereafter named iDH1 (Extended Data Fig. 1a). We found that 13 chemicals were able to rescue *crestin* expression independent of the DHODH inhibitor used (Supplementary Table 1).

We performed metabolite profiling by mass spectrometry on A375 melanoma cells to evaluate nucleotide and precursor levels 24 hours post treatment. Analysis revealed that hits fall into three classes. The first class affects the biochemical activity of leflunomide while the second class affects nucleotide pools. Chemicals of the third class bypass transcriptional defects through independent mechanisms (Fig. 1b–c, Extended Data Fig. 1b–c). Within this third group is the steroid hormone progesterone. Progesterone, an activator of Pgr, recued expression of the neural crest markers *crestin, sox10, pax3 and foxd3* (Fig. 1b, Extended Data Fig. 2a). We then tested whether progesterone also rescues neural crest defects

resulting from Paf complex deficiency. The Paf complex plays a crucial role in transcription elongation[11–13]. We found that progesterone circumvents aberrant transcription in *ctr9*[12] morphants and *paf1(aln*^{z24}*)*[14] mutants (Fig. 1d). This establishes that progesterone rescues elongation defects consequent to leflunomide or Paf complex deficiency.

To understand the developmental aspects of rescue, we added progesterone at varying times after leflunomide treatment. We found that 12 to 15 somites is the earliest stage to rescue neural crest (Extended Data Fig. 2b). We performed RNA-Seq on embryos treated with leflunomide, progesterone or both compounds at 8 and 15 somites. This captured transcriptional changes before onset and at emergence of the phenotype, respectively. Although DHODH inhibition is expected to lead to ubiquitous effects, different cell types may have varying sensitivities to inhibition depending on their ability to engage alternative mechanisms for nucleotide production, such as salvage pathways. Analysis of differentially expressed genes (DEGs) at 15 somites revealed that several lineages are likely affected by leflunomide, including muscle and skeletal systems (Supplementary Table 2). We additionally observed specific enrichment for neural crest-derived lineages. Mutations in DHODH cause Miller Syndrome, a human craniofacial disorder[15]. This highlights the susceptibility of neural crest to DHODH deficiency during development. Together, the data illustrate the tissue specific nature of gene expression defects with neural crest being prominently affected.

We observed little overlap (7%) in DEGs at 8 and 15 somites (Supplementary Table 2). We suspected neural crest effects to be obscured through bulk transcriptomic profiling of heterogeneous developing embryos. In order to resolve specific changes, we sorted *sox10*$^{+}$ neural crest cells at 15 somites from transgenic embryos treated with leflunomide, progesterone or both compounds (Extended Data Fig. 3a–b). Progesterone restores the gene signature imposed by leflunomide to near completion, rescuing over 83% of DEGs, including *foxd3* and *pax3* (Extended Data Fig. 3c, Supplementary Table 3). We observed a similar (72%) transcriptional reversion in *ctr9*-morphant *sox10*$^{+}$ cells (Extended Data Fig. 3d, Supplementary Table 4). Genes not rescued showed enrichment in developmental signaling pathways. We cannot exclude that these genes may require additional signals or time to restore their expression. Nonetheless, the data define progesterone as a strong chemical suppressor of leflunomide-mediated neural crest defects and supports a role for nuclear hormone signalling in overcoming transcriptional defects.

We verified *pgr* expression during early embryonic development by RT-PCR (Extended Data Fig. 4a). To test whether the effect of progesterone is mediated via its receptor, we abolished *pgr* expression using an ATG morpholino (MO). Embryos were treated with leflunomide or leflunomide plus progesterone, and *crestin* expression was assessed. We found that loss of *pgr* did not affect progesterone-mediated rescue. Rather, loss of *pgr* by itself was sufficient to rescue *crestin* upon leflunomide treatment (Fig. 2a). We ensured MO specificity through co-injection with wild-type (wt) or mismatched (7mm) *pgr* mRNA (Extended Data Fig. 4b). In line with the previous observation, *crestin* rescue was reduced by co-injection of the *pgr* MO with mismatched *pgr* mRNA (Fig. 2b). These data demonstrate that knockdown of *pgr* counteracts transcriptional defects arising from nucleotide depletion.

As *pgr* knockdown rescues neural crest, we hypothesized whether the progesterone dosage used in our studies decreased receptor expression through self-regulatory mechanisms. Effects of progesterone on PGR expression have been previously described in cancer[16,17]. We observed that progesterone reduced *pgr* levels by almost 2-fold in the embryos (Fig. 2c). These findings may explain why both exposure to progesterone and loss of its receptor yield the same biological effect *in vivo*. We also found that leflunomide increases *pgr* expression and were prompted to assess if *pgr* overexpression can mimic the effects of leflunomide. Overexpression of *pgr* was not sufficient to abrogate *crestin* expression (Extended Data Fig. 4c). This indicates that additional mechanisms are in play to establish loss of neural crest lineage through leflunomide. Together, the data support a function for Pgr during nucleotide stress.

To clarify the role of Pgr, we conducted co-immunoprecipitation (Co-IP) followed by mass spectrometry to identify complex interaction partners of the receptor. We injected embryos with *pgr:flag:T2A:gfp* mRNA and exposed them to DMSO, progesterone, or leflunomide plus progesterone prior to Co-IP at 15 somites. Amongst the top peptides identified was Hsp90, a known interactor of Pgr[18] (Fig. 2d, Supplementary Table 5). We found associations between Pgr and proteins from two major biological processes. First, Pgr associates with nucleotide metabolism enzymes such as Atic and Impdh2. This highlights a function for Pgr in the regulation of nucleotide levels. We also identified RNA metabolism proteins as potential complex partners of Pgr, including Ddx21. Ddx21 is an RNA helicase with reported functions in transcription and rRNA metabolism[19–21]. We verified the association between DDX21 and PGR in A375 cells with inducible PGR expression and in T47D cells where both proteins are expressed naturally (Fig. 2e, Extended Data Fig. 5a–b). This reveals an association between PGR and DDX21 in several cellular contexts.

Due to its regulating function in Pol I and Pol II transcription[19–21], we studied the role of Ddx21 *in vivo*. We confirmed *ddx21* expression during early development by RT-PCR (Extended Data Fig. 5c). We then knocked down *ddx21* using an ATG MO and exposed embryos to DMSO, leflunomide or iDH1. We observed that loss of *ddx21* rescues the neural crest upon leflunomide or iDH1 treatment (Fig. 3a–b). Co-injection of the MO with wild-type *ddx21* mRNA reduced rescue effects confirming MO specificity. Additionally, we assessed whether *crestin* rescue through loss of function recovers *in vivo* melanocyte differentiation potential. Pigmentation defects characterizing leflunomide-treated embryos are overcome by *ddx21* knock down (Fig. 3c). This establishes that knockdown of *ddx21* confers resistance to nucleotide depletion.

Ribosomal biosynthesis encompasses a significant demand for nucleotides. The rRNA of ribosomes is where the majority of nucleotides reside[22]. Given the dual function of DDX21 in regulating mRNA transcription and rRNA transcription, processing and modifications[23], we hypothesized that DDX21 responds to changes in nucleotide levels. To determine whether nucleotide depletion affects DDX21 binding to rRNA, we performed irCLIP for DDX21 in A375 cells after A77 1726 treatment. Remarkably, we observed that DDX21 binding to rRNA is reduced by nucleotide stress (Fig. 4a). Simultaneously, there is a significant increase in binding of DDX21 to mRNA, including 469 new bound transcripts (Fig. 4b, Supplementary Table 6). New DDX21-bound transcripts include mRNAs of genes

involved in pyrimidine metabolism and the cell cycle such as CAD and CDKN1A, respectively (Fig. 4c). The shift in DDX21 interaction from rRNA to mRNA is reversed by nucleotide supplementation, indicating this effect is specific to a reduction of nucleotide pools. We hypothesized that binding of DDX21 to mRNA affects corresponding protein levels. We therefore performed whole-proteomics analysis on A77 1726-treated A375 cells (Supplementary Table 7). We found no significant correlation between DDX21-bound mRNAs and their respective protein expression levels. Currently, the consequence of DDX21 binding to mRNAs is unknown. We do not exclude a role for DDX21 in mRNA processing during nucleotide stress. We conclude that nucleotide depletion leads to altered binding of DDX21 to mRNAs, but these changes are not reflected at protein levels of targeted transcripts.

Under homeostatic conditions, DDX21 is localized to the nucleolus where it directly binds rRNAs and snoRNAs[19,24]. Following transcriptional stress, DDX21 relocalizes to the nucleoplasm[19,20]. Based on our observation that DDX21 engages mRNAs during low nucleotide levels, we investigated whether DHODH inhibition affects DDX21 localization. We performed immunofluorescence (IF) staining for DDX21 in A375 cells 24 hours after A77 1726 treatment, the timepoint when nucleotide depletion is first observed[9]. We observed partial relocalization of DDX21 from the nucleolus to the nucleoplasm, which is reversed by nucleotide supplementation. No changes in total DDX21 protein levels were noted (Extended Data Fig. 6a–c). TCOF1, an unrelated nucleolar protein, did not display changes in localization upon nucleotide stress (Extended Data Fig. 6d–e). These observations reveal that DDX21 can interpret nucleotide levels and relocalizes to the nucleoplasm when nucleotide pools are limited.

Given that changes in DDX21 localization correlate with its chromatin occupancy[19], we investigated whether nucleotide stress affects DDX21 binding to chromatin. We performed ChIP-Seq for DDX21 and the CDK9 subunit of p-TEFb in A375 cells (Extended Data Fig.7a). Cells exposed to A77 1726 showed substantially reduced genomic occupancy of DDX21 and CDK9 compared to control cells. Remarkably, chromatin binding was re-established by the addition of nucleotides (Fig. 5a). Because of suggestions that DDX21 senses the transcriptional status of Pol I[21,25], we examined DDX21 occupancy in the 14kb rDNA repeat region. The data show that the genomic distribution of DDX21 along the rDNA genes for Pol I-directed transcripts is not affected by limited nucleotide pools (Extended Data Fig. 7b). However, we previously observed reduced binding of DDX21 to rRNA during nucleotide stress (Fig. 4a). Taken together, these observations suggest that the bulk effect of DDX21 in the nucleolus is reduced as well as the efficiency of ribosomal biogenesis. These data demonstrate that nucleotide depletion predominantly affects the activity of DDX21 on Pol II-mediated transcription and target genes.

To investigate if reduced genomic occupancy of DDX21 correlates with gene expression changes, we performed RNA-Seq 24 and 48 hours post A77 1726 treatment in A375 cells. We found that majority of transcriptional changes occur 48 hours after DHODH inhibition. More specifically, 32% of the genome was at least 2-fold downregulated while 17% of genes showed significant upregulation (Fig. 5b, Supplementary Table 8). Analysis of genes downregulated at 48 hours revealed high enrichment for genes involved in RNA metabolic

processes (Extended Data Fig. 8a). Nucleotide supplementation restores the gene signature imposed by A77 1726, indicating that the transcriptional changes originate from nucleotide stress (Fig. 5c).

We then compared DEGs at 48 hours to genes displaying reduced chromatin occupancy of DDX21 at 24 hours post A77 1726 treatment. We observed that 45% of the downregulated genes show loss of DDX21 binding during nucleotide depletion (Fig. 5d). Gene set analysis of downregulated DDX21 targets uncovers enrichment in genes associated with RNA metabolism and the cell cycle (Extended Data Fig. 8b). The data show that loss of DDX21 binding precedes transcriptional downregulation of genes such as CSTF2 (mRNA processing) and CCNB1 (cell cycle) under nucleotide stress. These observations could explain the transcriptional and proliferative defects seen in neural crest and melanoma after DHODH inhibition[1,9].

To test if loss of DDX21 and CDK9 from chromatin impacts promoter-proximal pausing, we performed PRO-Seq in A375 cells 24 hours post A77 1726 treatment[26]. Consistent with a broad increase in transcriptional pausing, we observed a genome-wide increase in signal at the promoter region. No changes within the gene body were found (Extended Data Fig. 8c–d). The PRO-Seq data suggests that the increased Pol II pausing that is occurring at 24 hours after treatment underlies the transcriptional downregulation seen at 48 hours. Due to its strong interaction with CDK9[19], we hypothesize that DDX21 sequesters CDK9 from chromatin following nucleotide depletion. This could drive the observed genome-wide loss of CDK9 under nucleotide stress. Consequent increases in Pol II pausing lead to transcriptional defects driving cell cycle arrest. In summary, limited nucleotide pools reduce expression of DDX21-bound genes.

Here, we employed an *in vivo* chemical suppressor screen in zebrafish to find drugs that confer resistance to DHODH-mediated nucleotide stress and subsequent transcriptional defects. While we do not distinguish between cell autonomous and non-cell autonomous effects of leflunomide, we consider both mechanisms to play a role. We found that alterations in progesterone and Pgr signalling lead to neural crest resilience when nucleotide pools are limited. Progesterone can bypass the elongation block induced by DHODH inhibition or Paf complex deficiency *in vivo*. We suggest that downregulation of Pgr reduces transcriptional activity of the receptor hereby ameliorating effects due to low abundance of nucleotides. We found that Pgr interacts with Ddx21 and propose that Ddx21 acts as a mediator between nuclear hormone signalling and the nucleotide stress response. Competition between the two signals could occur when both nucleotide stress and progesterone are present. *In vitro*, DDX21, together with CDK9, falls off chromatin to prevent transcription elongation when nucleotide levels are limited. Upon treatment with progesterone, DDX21 activity could be skewed toward its function in nuclear hormone signalling. We hypothesize that the presence of both progesterone and nucleotide depletion restores the interaction between DDX21 and CDK9 on chromatin thereby re-establishing efficient transcription and rescuing the neural crest lineage. Additionally, our study reveals a function for DDX21 as a sensor of nucleotide pools and mediator of transcription during nucleotide stress. DDX21 occupancy is lost at Pol II, but not Pol I (rDNA) targets when nucleotide pools are limited. This shows that polymerase I and II hold intrinsic differences in

their response to changes in nucleotide levels. While ribosomal genes are affected by nucleolar stress[20], cell cycle genes are affected by nucleotide stress through Pol II-mediated transcriptional effects. Patients undergoing chemotherapy regimens that target nucleotide metabolism often develop resistance[27]. Work in this study suggests that modulating DDX21 levels could be an attractive therapeutic strategy to delay disease progression.

Methods

Zebrafish handling

Zebrafish were handled according to the vertebrate animal protocol as approved by the Harvard University Animal Care Committee. Strains used are AB (wild-type) and *paf1(aln^{z24})* mutants.

Chemical screen and drug treatment

Wild-type zebrafish embryos were treated with leflunomide from 50% epiboly until 24 hours post-fertilization in E3 embryo media and fixed with 4% Formaldehyde. Chemical libraries screened: LOPAC (n= 1280), ICCBL (n= 480) and NIH clinical collection (n=450). Other chemical used include leflunomide (Sigma L5025), Progesterone (Sigma, P0130), Esomeprazole (Enzo life sciences), Aphidicolin (Enzo life sciences, BML-CC101–0001) and A77 1726 (Enzo Life Sciences, ALX-430–096-M025). For nucleotide rescue experiments, a cocktail of 10 μg/ml uridine 5′-monophosphate (Sigma, UMP) and 10 μg/ml cytidine 5′-monophosphate (Sigma, CMP) was added to A77 1726. For *in situ* hybridizations, we followed the methods as described by Thisse C, and Thisse, B[28,29].

Cell culture and generation of A375-iPRG (PRB) line

A375 cells (ATCC) and T47D cells (ATCC) were grown in DMEM or RPMI with 10% fetal bovine serum, 1X GlutaMAX and 1% Penicillin-Streptomycin. The full-length human PRB CDS was cloned into a pENTD (Life technologies) from a vector kindly provided by Brown Myles via Gateway recombination (Invitrogen). The primers used are F: caccATGACTGAGCTGAAGGCAAAGGG, R: CTTTTTATGAAAGAGAAGGGGTTTCAC (Supplementary Table 9). Subsequently PRB was subcloned to add a myc-tag using F: caccATGACTGAGCTGAAGGCAAAGGG, R: CTATAGTTCTAGAGGCTCGAGAG. The pENTD vector containing myc-tagged PRB was cloned into the pHage vector via Gateway recombination. Lentiviral particles were produced by co-transfection of 293T cells (ATCC) with sequence verified pHage-PRB and packaging plasmids pMD2.G (Addgene, #12259) and psPAX2 (Addgene #12260, gifts from Didier Trono), using FuGENE HD (Promega). Viral particles were harvested 48- and 72-hours post-transfection, concentrated by overnight PEG precipitation[30], resuspended in PBS, and stored at −80°C. A375 cells were overlaid with viral particles diluted in DMEM/1x Glutamax with 10% TET System Approved FBS (Clontech) and supplemented with 5 μg/ml polybrene (Sigma) for 24 hours at 37°C. 48 hours post-transduction, infected cells were selected with 500 μg/ml G418 (Gibco) for 7 days. Cell line is available upon request.

Targeted mass spectrometry and metabolite profile analyses

Targeted mass spectrometry and metabolite analysis were performed as previously described[9]. In short, samples were re-suspended using 20μL HPLC grade water. 5μL were injected and analysed using a hybrid 5500 QTRAP triple quadrupole mass spectrometer (AB/SCIEX) coupled to a Prominence UFLC HPLC system (Shimadzu) via selected reaction monitoring (SRM) [31]. Peak areas from the total ion current for each metabolite SRM transition were integrated using MultiQuant v2.0 software (AB/SCIEX). Spectral counts of metabolites were first normalized to the row average of the DMSO samples, followed by normalization to the median of the entire dataset.

cDNA cloning and *in vitro* transcription

Danio rerio Pgr cDNA was cloned into pENTR/D-TOPO (Thermo Fisher Scientific) using the following primers: F: CACCATGGACACGGTGAAC, R: CATCAGCGGTTTGACCATTCCTG. Final Destination vector cloning was performed using LR Clonase mix (Thermo Fisher Scientific) and 5'entry p5E-CMV/SP6 vector, 3'entry flag:bio:T2A:gfp vector and a pDestTol2CG2 backbone. The 7mm pgr construct was generated by NEB Q5 mutagenesis using pENTRD-pgr as a template and with the following primers: Q5_F:atacgtcccctgCTGATTCCACTGGGACGGTGACGGG, Q5_R: tgacggtatccatGGTGAAGGGGGCGGCCGC. hsDDX21 (wild-type) was subcloned using BamHI/XhoI into pCS2+ from the original plasmids provided by E. Calo[19]. Primers used: F:GTCAGGATCC**ATG**CCGGGAAAACTCC, R:CGTACTCGAGTCATCATTGACCAAATGCTT. mRNA was generated using mMESSAGE mMACHINE SP6 Transcription Kit (Life technologies). 1 nanoliter of mRNA mix was injected into 1-cell stage embryos.

Protein extracts Co-IP and mass spectrometry of zebrafish embryos

500 embryos were injected with *pgr:flag:T2A:gfp* mRNA, treated with the respective chemicals and collected at 15 somites. Embryos were checked for GFP expression, dechorionated, deyolked[32] and resuspended in Pierce IP Buffer. Anti-Flag M2 Magnetic beads (Sigma, M8823) were used to pull down Pgr:Flag proteins. Protein complexes were eluted using 3xFlag peptides (Sigma, F4799). Proteins were concentrated by TCA precipitation and loaded on a 10% acrylamide gel. Gel was stained with Colloidal Blue and excised bands were cut into 1 mm^3 pieces. Gel pieces were subjected to a modified in-gel trypsin digestion procedure[32]. Gel pieces were washed and dehydrated with acetonitrile for 10 minutes followed by removal of acetonitrile. Pieces were dried in a speed-vac. Rehydration of the gel pieces was done using 50 mM ammonium bicarbonate solution containing 12.5ng/μl modified sequencing-grade trypsin (Promega) at 4ºC. After 45 min, excess trypsin solution was removed and replaced with 50mM ammonium bicarbonate solution to cover the gel pieces. Samples were placed at 37ºC overnight. Peptides were extracted by removing the ammonium bicarbonate solution, followed by one wash with a solution containing 50% acetonitrile and 1% formic acid. The extracts were dried in a speed-vac and samples were stored at 4ºC. On the day of analysis, the samples were reconstituted in 5–10μl of HPLC solvent A (2.5% acetonitrile, 0.1% formic acid). A nano-scale reverse-phase HPLC capillary column was created by packing 2.6 μm C18 spherical silica beads into

a fused silica capillary (100 μm inner diameter x ~30 cm length) with a flame-drawn tip. After equilibrating the column each sample was loaded via a Famos auto sampler (LC Packings). A gradient was formed and peptides were eluted with increasing concentrations of solvent B (97.5% acetonitrile, 0.1% formic acid). As peptides eluted, they were subjected to electrospray ionization and entered into an LTQ Orbitrap Velos Pro ion-trap mass spectrometer. Peptides were detected, isolated, and fragmented to produce a tandem mass spectrum of specific fragment ions for each peptide. Peptide sequences were determined by matching to protein databases using Sequest software (v.28 (rev. 12). All databases include a reversed version of the sequences and the data was filtered to a 1–2% percent false discovery rate.

Co-immunoprecipitation (Co-IP)

Cells were washed twice with 1X PBS. Nuclei were isolated with 0.05% Triton in PBS and lysed in nuclei lysis buffer (20mM Hepes-KOH pH7.9, 25% glycerol, 420mM NaCl, 1.5mM MgCl2, 0.2mM EDTA, 0.5mM DTT). 500ug of protein extracts was used and the salt concentration was diluted from 420mM to 150mM NaCl using 20mM Hepes-KOH pH7.9, 20% glycerol, 0.25mM EDTA, 0.05% NP-40. Cell lysates were pre-cleared with non-antibody bounds beads for 1 hour at 4°C. Antibody bounds protein G Dynabeads were added to pre-cleared lysate and samples incubated overnight at 4°C. Antibodies used: IgG (Cell Signalling #2729), Progesterone Receptor B (C1A2), Cell Signalling #3157) and DDX21 (Novus Biologicals NB100–1718). Protein-bead complexes were then washed 5 times with wash buffer (20mM Hepes-KOH pH7.9, 10% Glycerol, 150mM NaCl, 1.5 MgCl2, 0.2mM EDTA, 0.5mM DTT) and beads were boiled in 50μL Laemmli Buffer for 15min at 95°C to elute proteins.

Western blotting and immunofluorescence stainings

A375 cells were treated for 24 hours, washed in 1X PBS, and collected in RIPA buffer with protease and phosphatase inhibitors. Samples were run on acrylamide gel and transferred onto a nitrocellulose membrane. Membrane was blocked for one hour in 5% of milk or TBS-T and incubated overnight at 4ºC with anti-DDX21 (Novus Biologicals NB100–1718, 1:3000), Progesterone Receptor B (C1A2), Cell Signalling #3157, 1:1000) or anti-actin (Abcam, ab14128, 1:1000). The next day, membranes were washed, incubated with HRP-conjugated secondary antibodies for 1 hour at RT, and developed with SuperSignal West Pico Plus Chemiluminescent substrate. DDX21 immunostaining was performed and quantified as described previously[19] using anti-DDX21 (NBP1–83310, 1:300) and anti-TCOF (NBP1–86909, 1:100). Images were acquired using an Andor Zyla VSC-04746 camera, calibrated at 1.63 μm/px, binning of 1×1 and an exposure of 70ms.

RNA extraction, RT-PCR and qRT-PCR

RNA isolation was performed using Trizol (Life Technologies, 15596–026) and the RNAeasy Kit (Qiagen). cDNA was synthesized with the Superscript Vilo cDNA synthesis kit (Life Technologies, 11754–050).

RT-PCR primers used:

Actin-F: ACCTCATGAAGATCCTGACC

Actin-R: TGCTAATCCACATCTGCTGG

Pgr#1-F: AAAGCTGCTACGACTCCACC

Pgr#1-R: AGACGACATGCGGGACAATT

Pgr#2-F: CAGACAGCATACACCGCATT

Pgr#2-R: GCTGTTGAGGAGGAGGTGAG

ddx21-F: ATCCAGCATGCCGTCAAAGA

ddx21-R: TCAAACAGGTACGAGACGCC

qPCR primers used:

bactin_F: CGAGCAGGAGATGGGAACC

bactin_R: CAACGGAAACGCTCATTGC

sox10_F: ATATCCGCACCTGCACAA

sox10_R: CGTTCAGCAGTCTCCACAG

crestin_F: AGTGCCTGCCAATGTTCAC

crestin_R: CTGAAAAAGGCCGATGAGTT

foxd3_F: CATGCAAAACAAGCCCAAG

foxd3_R: ATGAGGGCGATGTACGAGTAG

mitfa_F: GGCGGTTTAATATCAATGACAGA

mitfa_R: GGTGCCTTTATTCCACCTCA

snail2_F: TTATAGTGAACTGGAGAGTCCAACA

snail2_R: TCCATACTGTTATGGGATTGTACG

neurog1_F: CGTGCCATTATCTTCAACACA

neurog1_R: CGATCTCCATTGTTGATAACCTT

myf5_F: GCTACAACTTTGACGCACAAAA

myf5_R: CACGATGCTGGACAAACACT

qPCR_PGR#1_F: TTCTCGCTGGGTTGGAGAAC

qPCR_PGR#1_R: GCATAGCCAAGCAAAGGTCG

qPCR_PGR#2_F: CAGCATACACCGCATTCTCC

qPCR_PGR#2_R: ACCCTCAACAGCTGTCTTGA

Cell sorting and RNA-sequencing

300 embryos were treated with 7uM leflunomide, 16uM Progesterone or both drugs from 50% epiboly until 15 somites. Embryos were dechorionated with pronase and treated with Liberase. Sox10+ cells were sorted on a BD FACS aria II. 16.5ng of RNA from Sox10+ sorted cells was used for library preparation. For RNA-sequencing of zebrafish and human cells, isolated RNA was subjected to rRNA depletion (Zebrafish: RiboGone, Takara #634847, Human: Epicentre, RZG1224, MRZ11124C). For zebrafish: NGS libraries were generated using the Smarter Low Input and Low input library prep kits (Takara). For human: libraries were prepared using the NEBnext Ultra RNA library prep kit (NEB, E7530S). Libraries were sequenced on Illumina Hi-Seq2000. Quality control of RNA-Seq datasets was performed by FastQC and Cutadapt to remove adaptor sequences and low-quality regions. The high-quality reads were aligned to UCSC build danRer7 for zebrafish or hg19 for human using Tophat 2.0.11 without novel splicing form calls. Transcript abundance and differential expression were calculated with Cufflinks 2.2.1. FPKM values were used to normalize and quantify each transcript; the resulting list of differential expressed genes are filtered by log fold change > 1.

Morpholino injection and pgr overexpression

Morpholinos were obtained from Gene Tools, LLC, and injected into the yolk of 1-cell stage embryos with 2ng MO in 1nl volume. The ctr9 MO has been described by Bai, *et al*[33]. Morpholino sequences are:

ctr9 (NM_001083583): GATTTCAATGGATCCCCGAGACATG

pgr (NM_001166335.1): GGAGAAGTGTTCACCGTGTCCATTC

ddx21(ENSDART00000093149.5): ATTCTGGGAGACTCTTTGACGGCAT

100pg of wild-type *pgr:flag:T2A:gfp* mRNA (wild-type *pgr* mRNA) or mismatch *pgr:flag:T2A:gfp* mRNA containing 7 silent mutations (7mm *pgr* mRNA) was co-injected for MO experiments. For overexpression, 100pg of wild-type *pgr:flag:T2A:gfp* mRNA was injected.

ChIP-sequencing and analysis

ChIP-Seq was performed as previously described [9,34]. A375 cells were treated with 25μM DMSO, 25μM A771726 or 25μM A771726 plus nucleotides. After a 24 hours, cells were fixed in 1% formaldehyde and subjected to Co-IP using DDX21 (Novus Biologicals, NB100–1718) and Cdk9 (Santa Cruz, C-20) antibodies. Libraries were sequenced on Illumina Hi-Seq2000. All datasets were aligned to UCSC build version hg19 of the human genome using Bowtie2 (version 2.2.1) with the following parameters: --end-to-end, -N0, -

L20. We used the MACS2 version 2.1.0[35] peak finding algorithm to identify regions of ChIP-Seq peaks, with a q-value threshold of enrichment of 0.05 for all datasets. The genome-wide occupancy profile figures were generated by deeptools[36] using the reference-point mode and the scale-regions mode. The genomic distribution of DDX21 ChIP was plotted using the ChIPSeeker R package, annotatePeak to assign peaks to a genomic annotation, which includes whether a peak is in the TSS, Exon, 5' UTR, 3' UTR, Intronic or Intergenic. The genome annotation is from the R-bioconductor annotation packages. To map DDX21 ChIP-seq peak to the rDNA data, we followed published work[19]. Briefly, we obtained the DNA consensus sequence of the 43Kb ribosomal locus NCBI (GeneBank ID: U13369.1). Using the unique 43Kb region, we used Bowtie to map ChIP-seq reads with standard mapping parameters to the hg19 human genome build. Data was visualized with Integrative Genomics Viewer.

Infrared Crosslinking and Immunoprecipitation (irCLIP) and data analysis

irCLIP was performed as described[37]. DDX21 (Novus Biologicals, NB100–1718) bound to Protein G Dynabeads (Thermo Fisher Scientific) was used to IP for 8 hours at 4°C. irCLIP data was processed using the irCLIP pipeline (https://github.com/ChangLab/irCLIP/tree/lite). PCR duplicates were removed using unique molecular identifiers (UMI) in the RT primer region. Adapter and barcode sequences were trimmed, and reads were mapped step-wise to repetitive and then non-repetitive (GRCh38) genomes. Specific parameters used for the irCLIP pipeline are as follows: -f 18 (trims 17nt from the 5' end of the read), -l 16 (includes all reads longer than 16nt), –bm 29 (minimum MAPQ score from bowtie2 of 29 is required for mapping; unique mapping only), and –tr 2,3 (repetitive genome) and –tn 2,3 (non-repetitive genome) RT stop intersection (n,m; where n = replicate number and m = number of unique RT stops required per n replicates). Using the –tr/tn 2,3 parameters, a minimum of 6 RT stops are required to support any single nucleotide identified as crosslinking site.

Whole proteomics: Cell lysis, protein digest and TMT labeling mass spectrometry analysis

Cells were lysed by homogenization in lysis buffer (2% SDS, 150mM NaCl, 50mM Tris pH 7.4). Lysates were reduced with 5mM DTT, alkylated with 15mM iodoacetamide for 30 minutes in the dark, quenched with 50mM fresh DTT and proteins precipitated by methanol/chloroform precipitation. Digests were carried out in 200mM EPPS pH 8.5 in presence of 2% acetonitrile (v/v) with LysC (Wako, 2mg/ml at 1:75) for 3 hours at RT and subsequently trypsinated (Promega, #V5111, stock 1:75) overnight at 37°C. Missed cleavage rate was assayed from a small aliquot by mass spectrometry. For whole proteome analysis, digests containing 60μg of peptide material were directly labelled with TMT reagents. After quenching of TMT labelling reactions with hydroxylamine, TMT labelling reactions were mixed, solvent evaporated to near completion and TMT labelled peptides purified and desalted by acidic reversed phase C_{18} chromatography. Peptides were then fractionated by alkaline reversed phase chromatography into 96 fractions and combined into 12 samples. Before mass spectrometric analysis, peptides were desalted over Stage Tips[38]. Data were collected by a MultiNotch MS3 TMT method[39] using an Orbitrap Fusion Lumos mass spectrometer (Thermo Fisher Scientific) coupled to an EasynLC1200 HPL system (Thermo Fisher Scientific). The 100μm inner diameter capillary column used was packed with C_{18}

resin (SepPax Technologies Inc., 1.8μm). Peptides of each fraction were separated over 3 hours acidic acetonitrile gradients by LC prior to mass spectrometry (MS) injection. The first scan of the sequence was an MS1 spectrum (Orbitrap analysis; resolution 120,000; mass range 400−1400 Th). MS2 analysis followed collision-induced dissociation (CID, CE=35) with a maximum ion injection time of 150 ms and an isolation window of 0.7 Da. In order to obtain quantitative information, MS3 precursors were fragmented by high-energy collision-induced dissociation (HCD) and analyzed in the Orbitrap at a resolution of 50,000 at 200 Th. Further details on LC and MS parameters and settings used were described recently[40]. Peptides were searched with a SEQUEST (v.28, rev. 12) based software against the human proteome (Uniprot 02/2014) with added common contaminant proteins. For this, spectra were first converted to mzXML. Searches were performed using a mass tolerance of 50 ppm for precursors, fragment ion tolerance 0.9Da to maximize sensitivity in conjunction with SEQUEST searches and linear discriminant analysis. For the searches maximally 2 missed cleavages per peptide were allowed. We searched dynamically for oxidized methionine residues (+15.9949 Da) and applied a target decoy database strategy and a false discovery rate (FDR) of 1% set for peptide-spectrum matches following filtering by linear discriminant analysis (LDA) and a final collapsed protein-level FDR of 1%. Quantitative information on peptides was derived from MS3 scans. Quant tables were generated requiring an MS2 isolation specificity of >65% for each peptide and a sum of TMT s/n of >150 over all channels for any given peptide and exported to Excel and further processed therein. Details of the TMT intensity quantification method and further search parameters applied were described recently[40].

PRO-Seq Analysis

Cells were collected, washed with PBS and washed with wash buffer (10mM Tris-Cl, pH 8.0, 10mM KCl, 250mM sucrose, 5mM MgCl2, 0.5mM DTT, 10% Glycerol). Cells were permeabilized with 0.1% Igepal for 2 minutes at RT, spun and resuspended in freezing buffer (50mM Tris-CL pH 8.3, 40% glycerol, 5mM MgCl2, 0.5mM DTT). Nuclei were counted, and flash frozen. PRO-Seq libraries were generated using 1 million nuclei per sample. Samples were spiked with 40,000 Drosophila S2 cells as normalization control. Samples were sequenced on the NextSeq using a High Output 75-cycle kit to an average depth of 10 million mappable reads per sample. To remove adapter sequence and low quality 3’ ends, we used cutadapt 1.14 to discard reads shorter than 20nt (-m 20 -q 10), and removing a single nucleotide from the 3’ end of all trimmed reads to allow successful alignment with Bowtie 1.2.2. Remaining read pairs were aligned to the Drosophila Dm3 genome index to determine spike-normalization ratios based on uniquely mapped reads. Counts of pairs mapping uniquely to spike-in RNAs were determined for each sample. Depth normalization was used for each bedGraph. Reads mapped to dm3 were excluded from further analysis, and unmapped pairs were aligned to the human hg19 genome. Identical parameters were utilized in each alignment described above (-m1, -v2, -X1000, --un). Pairs mapping uniquely to hg19, representing biotin-labeled RNAs were separated, and strand-specific counts of the 3’-end mapping positions determined at single nucleotide resolution, genome-wide, and expressed in bedGraph format with “plus” and “minus” strand labels, as appropriate. Combined bedGraphs were generated after deduplication by summing counts per nucleotide of all 3 replicates for each condition. Read counts were calculated per

gene (from transcription start site to transcription end site), in a strand-specific manner, based on default annotations (Ensembl hg19), using feature Counts. Differentially expressed genes were identified using DESeq2 v1.18.1 under R 3.3.1. PRO-Seq size factors were determined based on spike normalization (for Control: 1.401, 1.365, 1.422; drug-treated: 0.973, 1.158, 0.832; rescued: 1.225, 1.805, 1.089). At an adjusted p-value threshold of $p<0.05$, 3135 affected genes were identified in A77 1726 treated cells and 2 affected genes in A77 1726 plus nucleotides treated cells, as differentially expressed compared to A375 control cells. UCSC Genome Browser tracks were generated from the combined replicates per condition, normalized as in the differential expression analysis.

Statistics and Reproducibility

Bar graphs represent mean ± s.d. for $n = 3$ or more independent experiments. Box plots represent median with minima and maxima (relocalization assay) or median with 10^{th} and 90^{th} percentiles (PRO-Seq) for $n = 3$ experiments. Significance was calculated using two-way ANOVA with Bonferri correction (metabolimics assay), unpaired T-test with Welch correction (*pgr* qPCR), two-sided Wilcoxon–Mann–Whitney test (relocalization assay), hypergeometric Test (ChIP-seq to RNA-seq overlap) and hypergeometric test and Benjamini-Hochberg correction (Gene Ontology analysis). All statistical analysis was performed using GraphPad Prism 5 (GraphPad Software). For qPCR of sorted $sox10^{+}$-GFP cells in Extended Data Fig. 3b. The data is from one independent experiment due to limited material. For RT-PCR of *pgr* during early development in Extended Data Fig. 4a. This data is from one independent experiment as *pgr* expression during early zebrafish development has been verified previously assessed through *in situ* hybridization and single-cell RNA-seq in zebrafish embryos by Bertrand, *et al.* [41] and Wagner, *et al.* [42], respectively.

Data availability

Deep-sequencing (ChIP-seq, RNA–seq, PRO-seq, irCLIP) data that support the findings of this study have been deposited in the Gene Expression Omnibus (GEO) under accession code GSE128086. Mass spectrometry data have been deposited in ProteomeXchange with the primary accession code PXD014433. All other data supporting the findings of this study are available from the corresponding author on reasonable request.

Reporting summary

Further information on research design is available in the Nature Research Reporting Summary linked to this article.

Extended Data

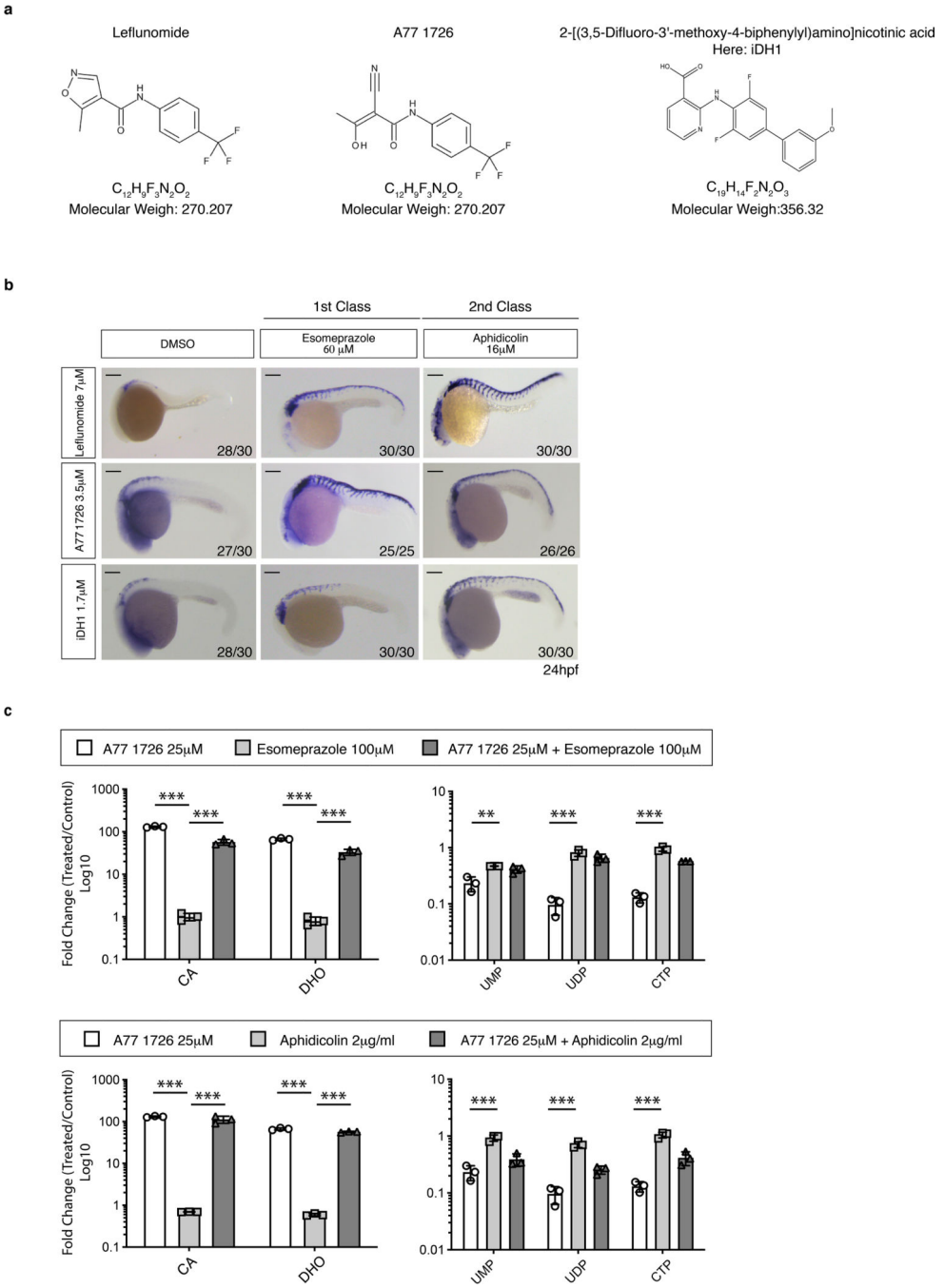

Extended Data Fig. 1. A chemical suppressor screen for Leflunomide

(a) Chemical structure of the Leflunomide, the active metabolite of leflunomide known as A77 1726 and an the independent DHODH inhibitor named here iDHODH1, or iDH1. (b) Lateral view of embryos at 24hpf treated with chemicals as indicated and subjected to *in situ* hybridization for *crestin*. Number of embryos displaying the indicated phenotype is indicated in the lower right corner. Scale bars represent 200µm. (c) Metabolite profiling in A375 melanoma cells. Upper panel: A375 cells exposed to A77 1726, Esomeprazol or both compounds for 24 hours. Lower panel: cells exposed to A77 1726, Aphidicolin or both

chemicals. (n = 3 independent experiments, Mean ± SD, Two-Way ANOVA with Bonferroni Comparison, ** = $p < 0.01$, *** = $p < 0.0001$). Source data are available online.

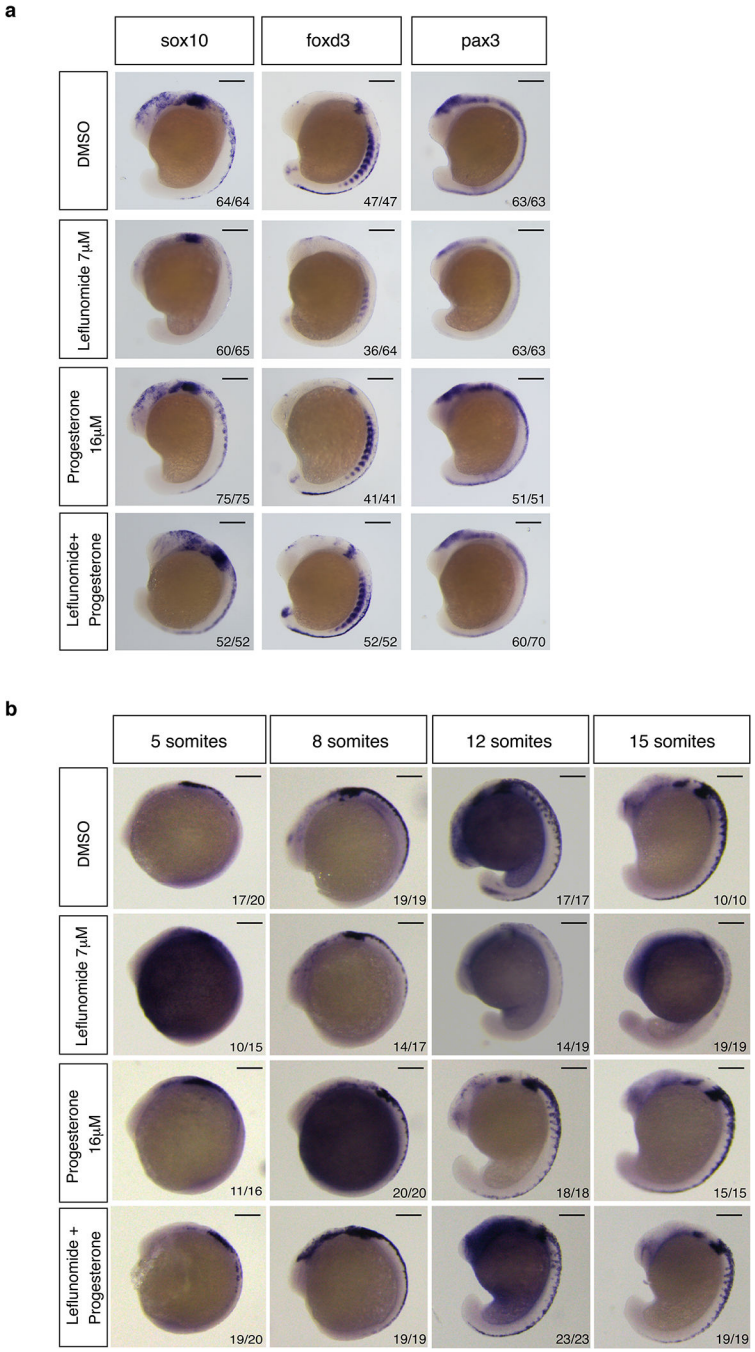

Extended Data Fig. 2. Effects of Leflunomide and Progesterone on neural crest during embryonic development.

(a) *In situ* hybridization for the neural crest cell markers *sox10, foxd3 and pax3* in zebrafish embryos at the 15-somite stage upon treatment with indicated chemicals. (b) Lateral view of embryos subjected to *in situ* hybridization for *crestin* at 5, 8, 12 and 15 somites. Number of embryos displaying the presented phenotype is indicated in lower right corner. Scale bars represent 200μm.

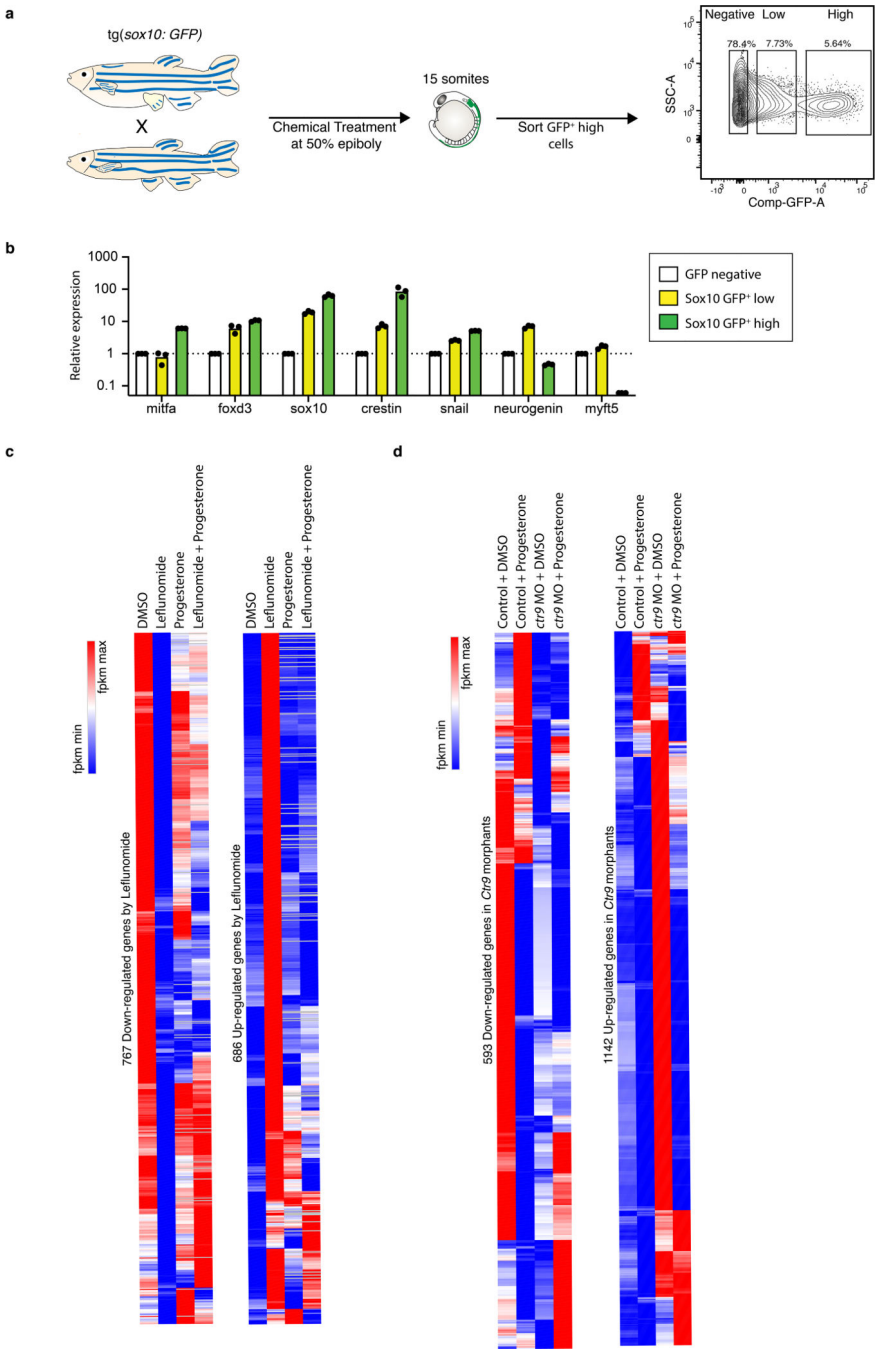

Extended Data Fig. 3. Progesterone restores transcriptional changes caused by DHODH inhibition.

(a) Schematic representation workflow to sort neural crest cells, here defined as *sox10*:GFP positive cells. (b) qPCR on whole embryos, sorted GFP low and sorted GFP high neural crest cells for neural crest *(mitfa, foxd3, sox10, crestin, snail2)* and non-neural crest (*neurogenin and myf5)* genes (n = 3 technical replicates, pooled from 1 experiment, Mean ± SD). (c, d) Hierarchical clustering heatmap of genes down-regulated or up-regulated in *sox10*:GFP high cells sorted from leflunomide-treated zebrafish (c) or *ctr9* morphants (d).

Differentially expressed genes criteria: log2 fold change ≥ 1.5 or ≤ 1.5. (n = 3 biologically independent experiment). Source data are available online.

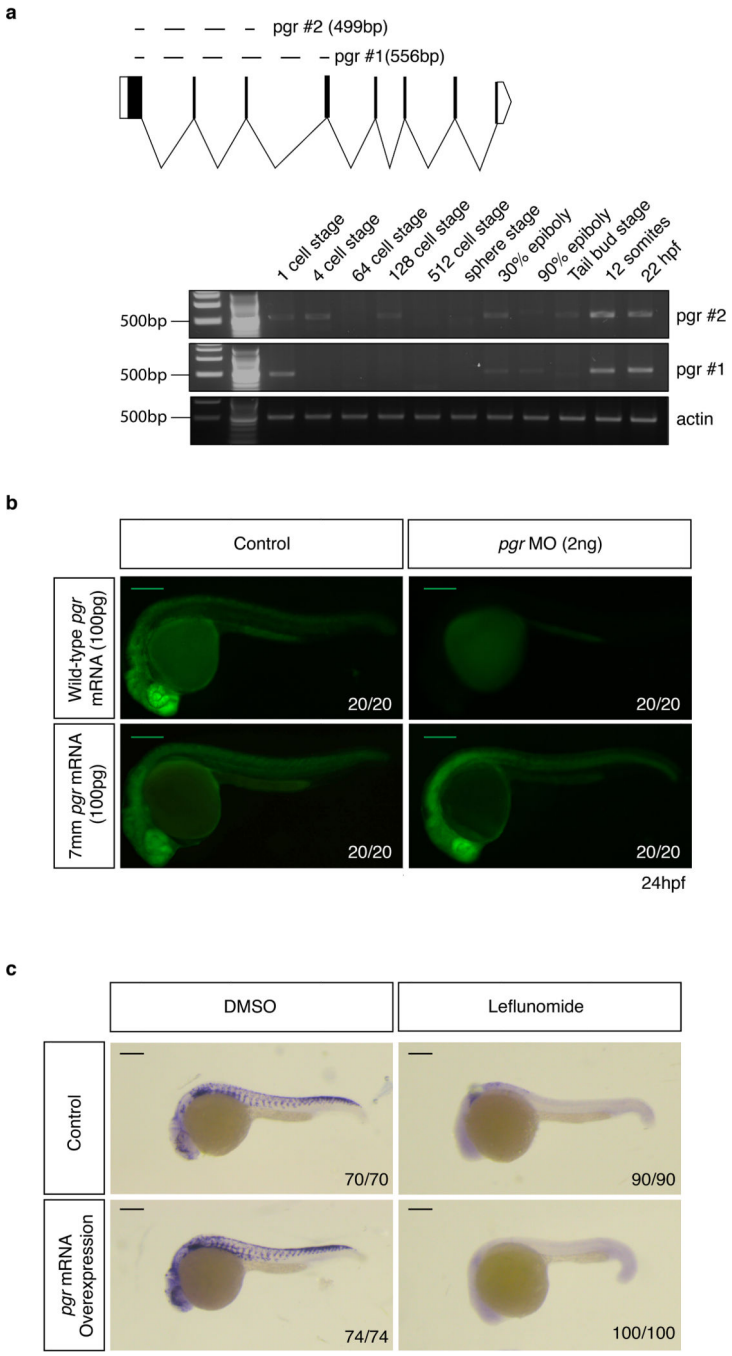

Extended Data Fig. 4. Progesterone receptor expression and perturbation effects.

(a) RT-PCR for *pgr* using two primer sets to reveal receptor expression during early development (1 experiment). (b) GFP positive embryos injected with *pgr:flag:T2A:gfp* mRNA or mismatched *pgr* mRNA with a *pgr* morpholine (MO) reveals MO specificity. Scale bars represent 200μm. (c) *In situ* hybridization for *crestin* at 24hpf in control and *pgr* mRNA injected embryos with or without leflunomide treatment. Number of embryos displaying the phenotype represented is indicated. Scale bars represent 200μm.

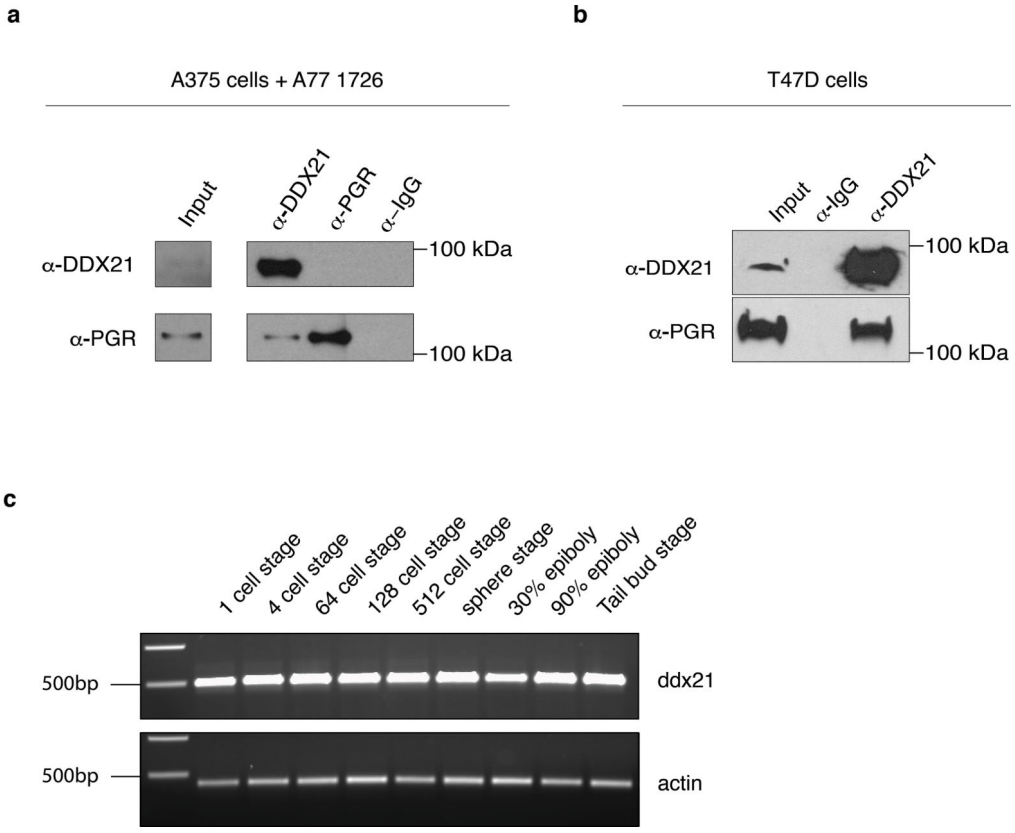

Extended Data Fig. 5. DDX21 interacts with PGR and loss of *pgr* function rescues *crestin* expression *in vivo*.

(a, b) DDX21 associates with PGR in A375 melanoma cells containing a doxycycline inducible PGR expression and in T47D breast cancer cells (2 independent biological experiments per cell line). (c) RT-PCR for *ddx21* to reveal receptor expression during early development (3 independent experiments). Source data are available online.

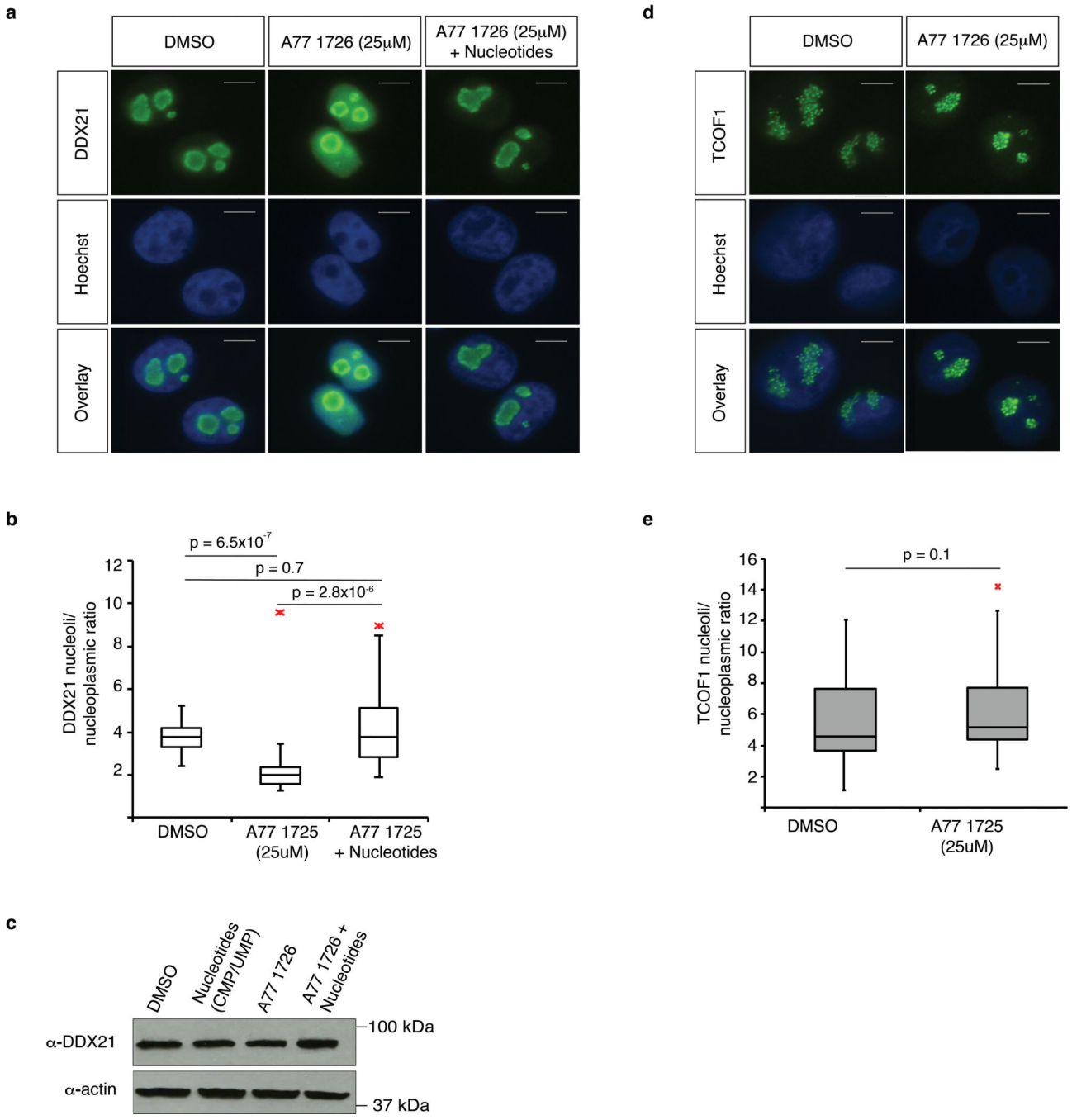

Extended Data Fig. 6. DDX21 relocalizes from the nucleolus to the nucleoplasm upon nucleotide depletion.

(a, d) DDX21 and TCOF1 immunofluorescence staining in A375 melanoma cells. Experiment was 4 times repeated independently with similar results. Scale bar represents 100μm. (b, e) Quantification of nucleoli to nucleoplasm ratio (n = 5 sections per condition, Two-sided Wilcoxon-Mann-Whitney test). Box plots represent median value and 25th and 75th percentiles. Whiskers are minima and maxima. Red asterisks indicate outliers. (c) Western blot analysis for DDX21 in A375 cells treated for 24 hours with DMSO, A77 1726

or A77 1726 plus nucleotides. Actin was used as loading control. Immunoblot are representative of at least 2 independent experiments. Source data are available online.

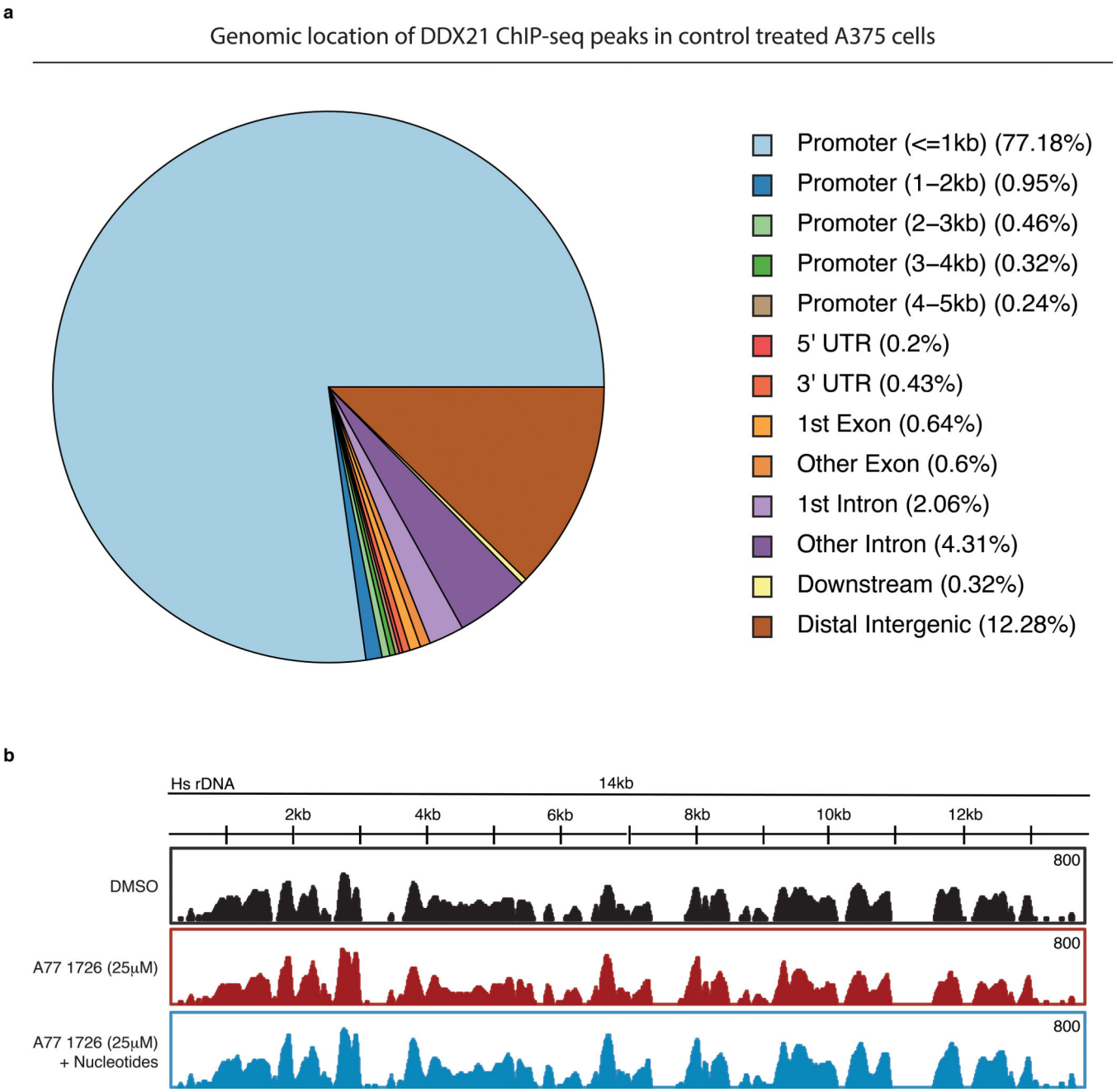

Extended Data Fig. 7. Genome wide annotation for DDX21 bound regions in A375 cells.

(a) Pie chart indicating the location of DDX21 ChIP-Seq peaks relative to gene locations in A375 melanoma cells treated with DMSO for 24hrs. (b). Gene track of DDX21 binding at 14kb rDNA region in A375 melanoma cells treated for 24 hours with DMSO, A77 1726 or and A77 1726 plus nucleotides. Source data are available online.

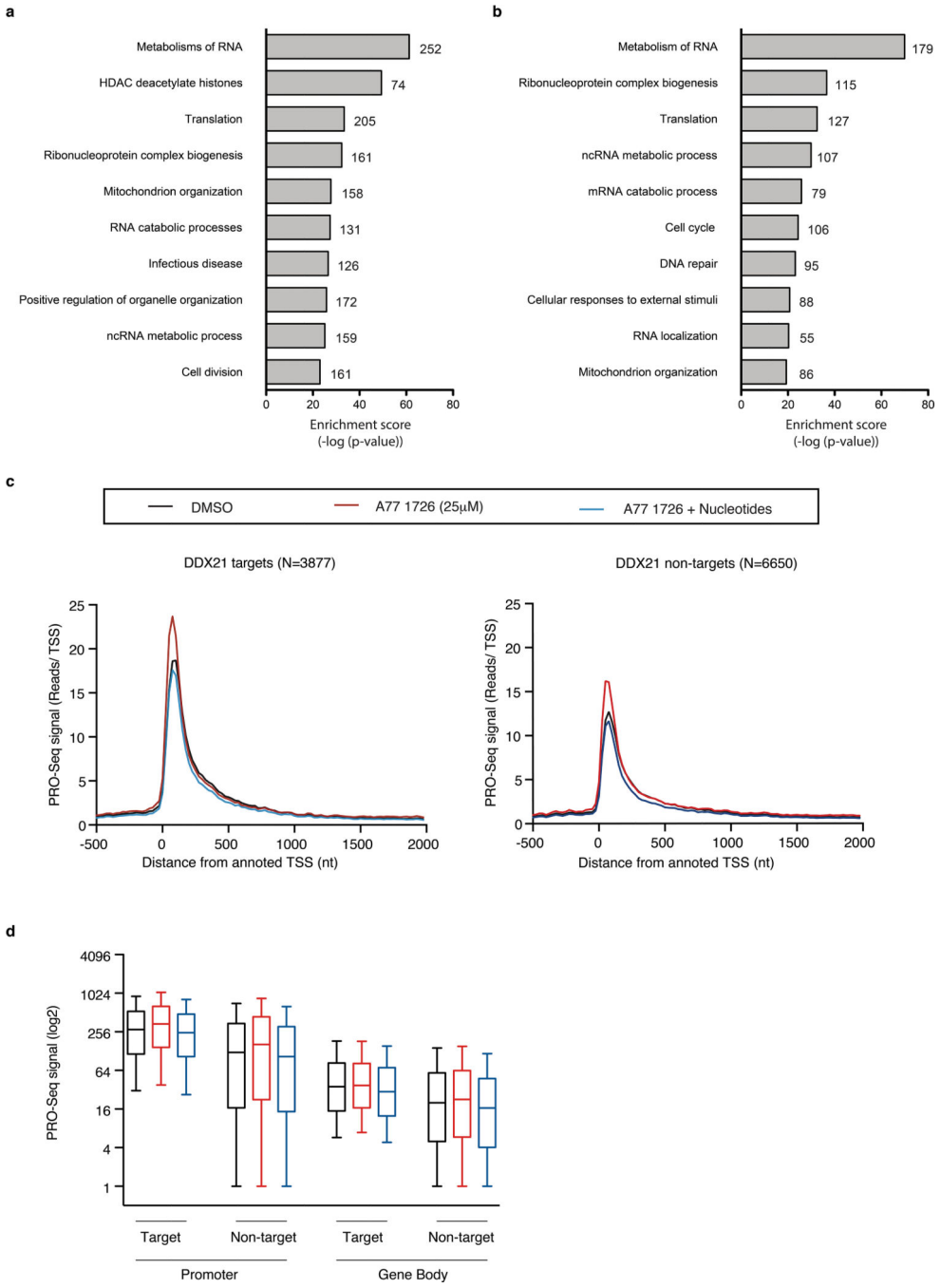

Extended Data Fig. 8. Gene Ontology analysis and PRO-Seq analysis in A375 cells.

Gene Ontology (GO) term enrichment analysis of genes down-regulated (a) and down-regulated DDX21 target genes (b) in A375 melanoma cells 48 hours post treatment with A77 1726 (n = 3 independent biological experiments, hypergeometric test and Benjamini-Hochberg correction). The number of genes associated to each GO term is shown at the end of each bar within the graph. (c) PRO-seq in A375 cells. Nascent transcription at the transcription start site (TSS) and at the gene body of DDX21 target and not-DDX21 target genes in cells treated for 24hrs with DMSO, A77 1726 or A77 1726 plus nucleotides (n = 3

biologically independent experiments). (d) Box plot of PRO-Seq signal shows no difference of nascent transcription in DDX21-bound and non-bound genes, as no changes are observed in promoter to gene body ratio between DDX21 targets and non-targets. Box plots represent median value and 25th and 75th percentiles. Whiskers are 10th and 90th percentile (n = 3 biologically independent experiments). Source data are available online.

Supplementary Material

Refer to Web version on PubMed Central for supplementary material.

Acknowledgments

We thank the following for their support and contribution: E. Fast, A. Choudhuri, and J.M. Ordovas-Montanes for critical reading of our manuscript; M. Rossman, E. Patton, J. Johansson, R. A. Young, and J. Wysocka for discussions about the project; B. Miles, L. Krug, D. Grunwald, S. Spengler, M. Yuan, J. Asara, L. Rubin, A. Avanites, and T. Schlaeger for help with reagents and experiments. This work was supported by NIH grant P50-GM107618 (M.K.), the Hope Funds for Cancer Research (B.J.A.) and the following grants from L.I.Z: Cancer Biology R01 CA103846, NIH Melanoma PPG, P01CA63222, Melanoma Research Alliance, Starr Cancer Consortium grant.

References

1. White RM et al. DHODH modulates transcriptional elongation in the neural crest and melanoma. Nature 471, 518–522 (2011). [PubMed: 21430780]
2. Lane AN & Fan TW-M Regulation of mammalian nucleotide metabolism and biosynthesis. Nucleic Acids Res. 43, 2466–2485 (2015). [PubMed: 25628363]
3. Chabosseau P et al. Pyrimidine pool imbalance induced by BLM helicase deficiency contributes to genetic instability in Bloom syndrome. Nature Communications 2, 368–6 (2011).
4. Liu W et al. Reprogramming of proline and glutamine metabolism contributes to the proliferative and metabolic responses regulated by oncogenic transcription factor c-MYC. Proc. Natl. Acad. Sci. U.S.A 109, 8983–8988 (2012). [PubMed: 22615405]
5. Guo J & Price DH RNA polymerase II transcription elongation control. Chemical Reviews 113, 8583–8603 (2013). [PubMed: 23919563]
6. Gressel S et al. CDK9-dependent RNA polymerase II pausing controls transcription initiation. eLife 6, R106 (2017).
7. Peng J, Liu M, Marion J, Zhu Y & Price DH RNA polymerase II elongation control. Cold Spring Harb. Symp. Quant. Biol 63, 365–370 (1998). [PubMed: 10384301]
8. Adelman K & Lis JT Promoter-proximal pausing of RNA polymerase II: emerging roles in metazoans. Nat. Rev. Genet 13, 720–731 (2012). [PubMed: 22986266]
9. Tan JL et al. Stress from Nucleotide Depletion Activates the Transcriptional Regulator HEXIM1 to Suppress Melanoma. Mol. Cell 62, 34–46 (2016). [PubMed: 27058786]
10. Luo R, An M, Arduini BL & Henion PD Specific pan-neural crest expression of zebrafish Crestin throughout embryonic development. Dev. Dyn 220, 169–174 (2001). [PubMed: 11169850]
11. Jurynec MJ et al. The Paf1 Complex and P-TEFb have reciprocal and antagonist roles in maintaining multipotent neural crest progenitors. Development dev.180133 (2019). doi:10.1242/dev.180133
12. Akanuma T, Koshida S, Kawamura A, Kishimoto Y & Takada S Paf1 complex homologues are required for Notch-regulated transcription during somite segmentation. EMBO Rep. 8, 858–863 (2007). [PubMed: 17721442]
13. Yoo H-S, Seo J-H & Yoo J-Y CTR9, a component of PAF complex, controls elongation block at the c-Fos locus via signal-dependent regulation of chromatin-bound NELF dissociation. PLoS ONE 8, e61055 (2013). [PubMed: 23593388]

14. Cretekos CJ & Grunwald DJ alyron, an insertional mutation affecting early neural crest development in zebrafish. Developmental Biology 210, 322–338 (1999). [PubMed: 10357894]
15. Rainger J et al. Miller (Genee-Wiedemann) syndrome represents a clinically and biochemically distinct subgroup of postaxial acrofacial dysostosis associated with partial deficiency of DHODH. Hum. Mol. Genet. 21, 3969–3983 (2012). [PubMed: 22692683]
16. Read LD, Snider CE, Miller JS, Greene GL & Katzenellenbogen BS Ligand-modulated regulation of progesterone receptor messenger ribonucleic acid and protein in human breast cancer cell lines. Molecular Endocrinology 2, 263–271 (1988). [PubMed: 3398853]
17. Diep CH, Ahrendt H & Lange CA Progesterone induces progesterone receptor gene (PGR) expression via rapid activation of protein kinase pathways required for cooperative estrogen receptor alpha (ER) and progesterone receptor (PR) genomic action at ER/PR target genes. Steroids 114, 48–58 (2016). [PubMed: 27641443]
18. Botos J, Xian W, Smith DF & Smith CL Progesterone receptor deficient in chromatin binding has an altered cellular state. J. Biol. Chem 279, 15231–15239 (2004). [PubMed: 14744870]
19. Calo E et al. RNA helicase DDX21 coordinates transcription and ribosomal RNA processing. Nature 518, 249–253 (2015). [PubMed: 25470060]
20. Calo E et al. Tissue-selective effects of nucleolar stress and rDNA damage in developmental disorders. Nature 554, 112–117 (2018). [PubMed: 29364875]
21. Xing Y-H et al. SLERT Regulates DDX21 Rings Associated with Pol I Transcription. Cell 169, 664–678.e16 (2017). [PubMed: 28475895]
22. Valvezan AJ et al. mTORC1 Couples Nucleotide Synthesis to Nucleotide Demand Resulting in a Targetable Metabolic Vulnerability. Cancer Cell 32, 624–638.e5 (2017). [PubMed: 29056426]
23. Sarkar M & Ghosh MK DEAD box RNA helicases: crucial regulators of gene expression and oncogenesis. Front Biosci (Landmark Ed) 21, 225–250 (2016). [PubMed: 26709771]
24. Sloan KE et al. The association of late-acting snoRNPs with human pre-ribosomal complexes requires the RNA helicase DDX21. Nucleic Acids Res. 43, 553–564 (2015). [PubMed: 25477391]
25. Song C, Hotz-Wagenblatt A, Voit R & Grummt I SIRT7 and the DEAD-box helicase DDX21 cooperate to resolve genomic R loops and safeguard genome stability. Genes & Development 31, 1370–1381 (2017). [PubMed: 28790157]
26. Kwak H, Fuda NJ, Core LJ & Lis JT Precise maps of RNA polymerase reveal how promoters direct initiation and pausing. Science 339, 950–953 (2013). [PubMed: 23430654]
27. Luengo A, Gui DY & Vander Heiden MG Targeting Metabolism for Cancer Therapy. Cell Chem Biol 24, 1161–1180 (2017). [PubMed: 28938091]

Methods References

28. Thisse C & Thisse B High-resolution in situ hybridization to whole-mount zebrafish embryos. Nat Protoc 3, 59–69 (2008). [PubMed: 18193022]
29. Thisse B & Thisse C In situ hybridization on whole-mount zebrafish embryos and young larvae. Methods Mol. Biol 1211, 53–67 (2014). [PubMed: 25218376]
30. Kutner RH, Zhang X-Y & Reiser J Production, concentration and titration of pseudotyped HIV-1-based lentiviral vectors. Nat Protoc 4, 495–505 (2009). [PubMed: 19300443]
31. Yuan M, Breitkopf SB, Yang X & Asara JM A positive/negative ion-switching, targeted mass spectrometry-based metabolomics platform for bodily fluids, cells, and fresh and fixed tissue. Nat Protoc 7, 872–881 (2012). [PubMed: 22498707]
32. Link V, Shevchenko A & Heisenberg C-P Proteomics of early zebrafish embryos. BMC Dev. Biol 6, 1–9 (2006). [PubMed: 16412219]
33. Bai X et al. TiF1-gamma plays an essential role in murine hematopoiesis and regulates transcriptional elongation of erythroid genes. Developmental Biology 373, 422–430 (2013). [PubMed: 23159334]
34. Batsché E, Yaniv M & Muchardt C The human SWI/SNF subunit Brm is a regulator of alternative splicing. Nature Structural & Molecular Biology 13, 22–29 (2006).

35. Zhang Y et al. Model-based analysis of ChIP-Seq (MACS). Genome Biol. 9, R137–9 (2008). [PubMed: 18798982]

36. Ramírez F et al. deepTools2: a next generation web server for deep-sequencing data analysis. Nucleic Acids Res. 44, W160–5 (2016). [PubMed: 27079975]

37. Zarnegar BJ et al. irCLIP platform for efficient characterization of protein-RNA interactions. Nature Methods 13, 489–492 (2016). [PubMed: 27111506]

38. Rappsilber J, Friesen WJ, Paushkin S, Dreyfuss G & Mann M Detection of arginine dimethylated peptides by parallel precursor ion scanning mass spectrometry in positive ion mode. Anal. Chem. 75, 3107–3114 (2003). [PubMed: 12964758]

39. McAlister GC et al. MultiNotch MS3 enables accurate, sensitive, and multiplexed detection of differential expression across cancer cell line proteomes. Anal. Chem 86, 7150–7158 (2014). [PubMed: 24927332]

40. Paulo JA et al. Quantitative mass spectrometry-based multiplexing compares the abundance of 5000 S. cerevisiae proteins across 10 carbon sources. J Proteomics 148, 85–93 (2016). [PubMed: 27432472]

41. Bertrand S et al. Unexpected novel relational links uncovered by extensive developmental profiling of nuclear receptor expression. PLoS Genet. 3, e188 (2007). [PubMed: 17997606]

42. Wagner DE et al. Single-cell mapping of gene expression landscapes and lineage in the zebrafish embryo. Science 360, 981–987 (2018). [PubMed: 29700229]

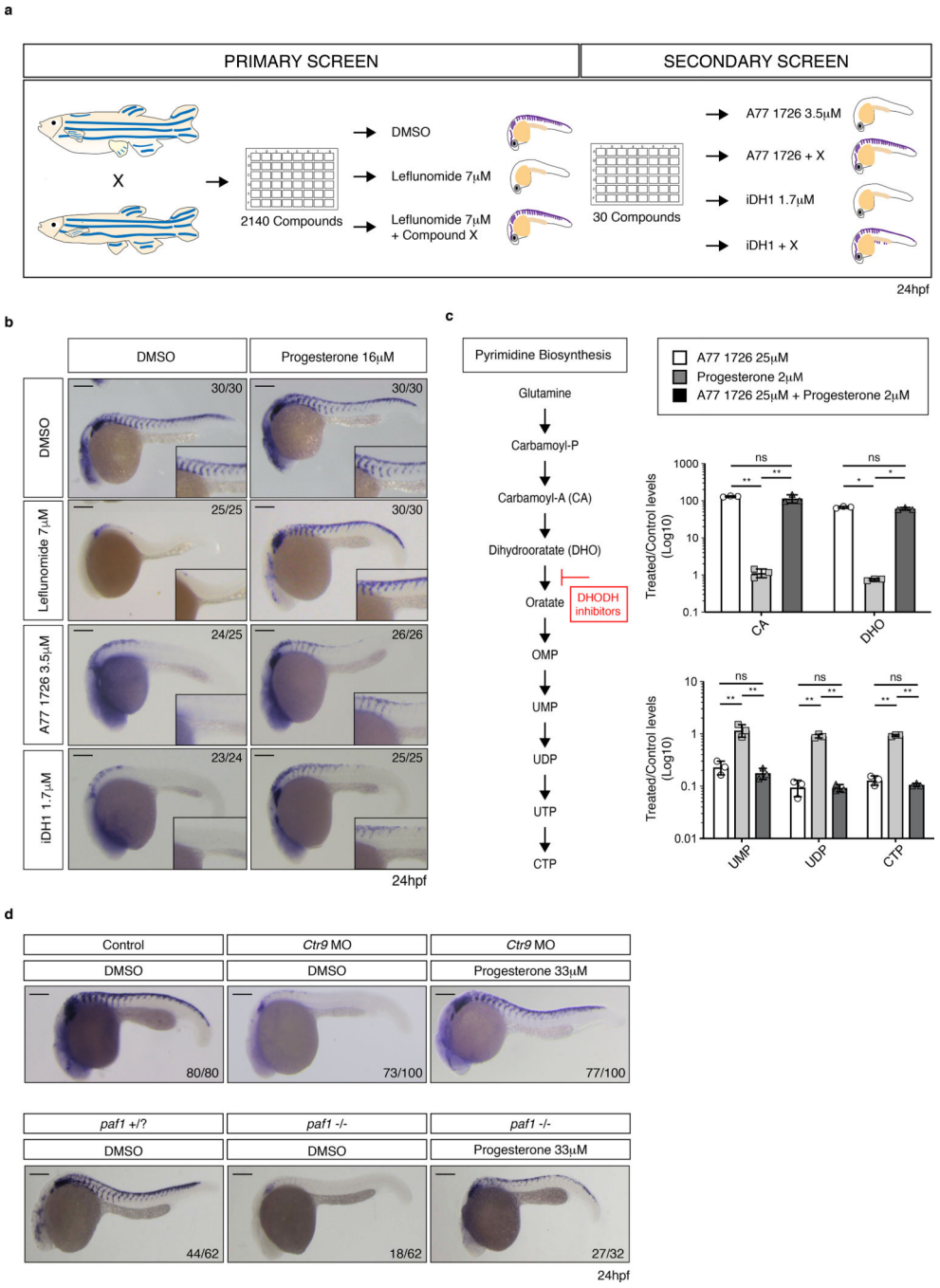

Figure 1. Progesterone confers resistance to nucleotide depletion *in vivo*.

(a) Schematic overview of chemical suppressor screen performed in zebrafish embryos with the DHODH inhibitors leflunomide, A77 1726, and iDHODH1 (iDH1). *Crestin* expression was assessed at 24hpf. (b) *In situ* hybridization for *crestin* at 24hpf in embryos treated with the indicated DHODH inhibitors plus or minus progesterone. Number of embryos displaying the represented phenotype is noted. Scale bar represents 200μm. (c) Pyrimidine biosynthesis pathway highlighting the enzymatic conversion inhibited by the leflunomide, A77 1726 and iDH1. Metabolite profiling of A375 melanoma cells exposed to indicated chemicals for 24

hours. (n = 3 biologically independent experiments, Mean ± SD, Two-Way ANOVA with Bonferroni Comparison, * = $p < 0.001$, ** = $p < 0.0001$, ns = $p > 0.05$). (d) *In situ* hybridization for *crestin* at 24hpf in *Ctr9* morpholine (MO) injected or *paf* mutant zebrafish embryos exposed to DMSO or progesterone. Number of embryos displaying the presented phenotype is indicated. Scale bars represent 200μm. Source data are available online.

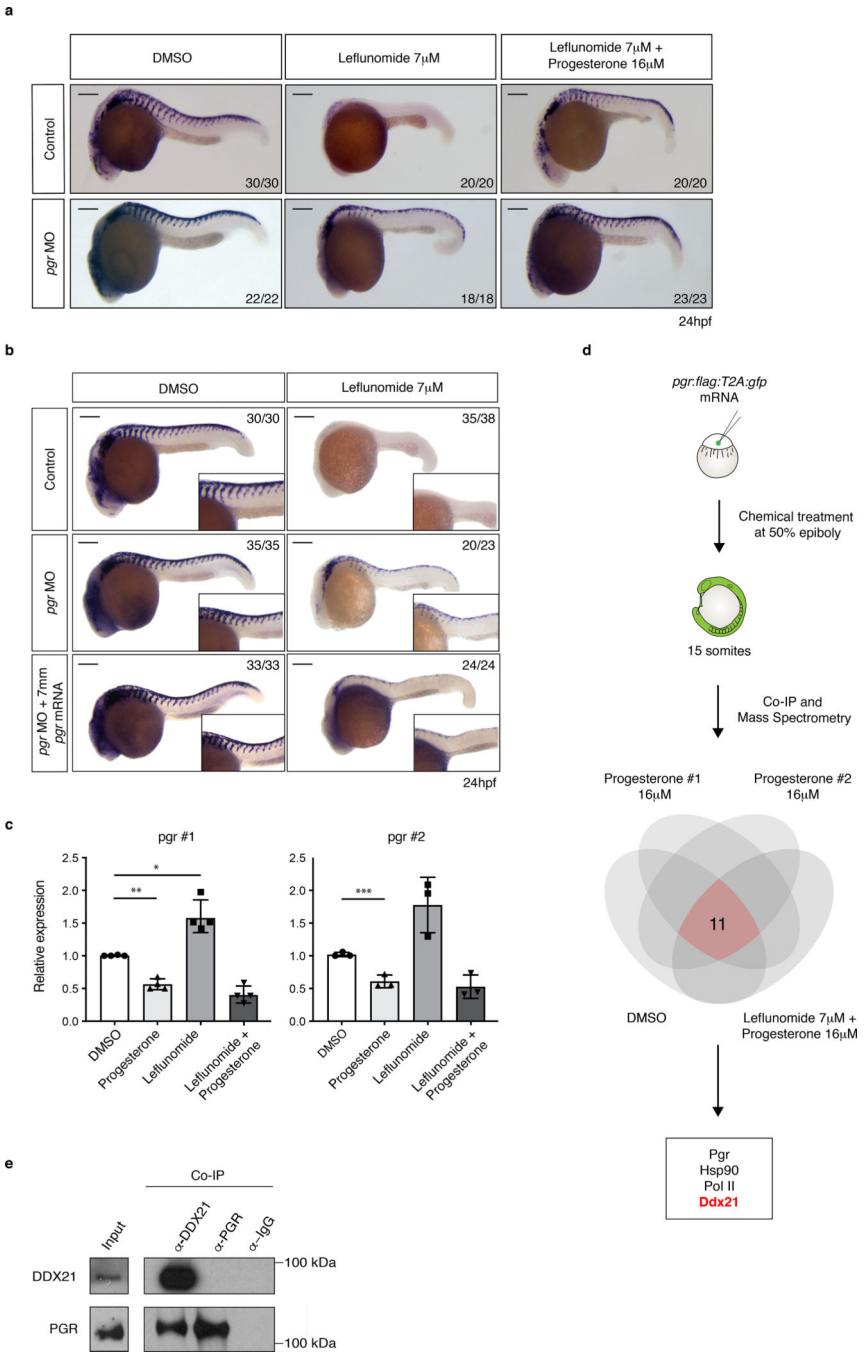

Figure 2. The progesterone receptor interacts with RNA-helicase DDX21.

(a, b) *In situ* hybridization at 24hpf for *crestin* in control, *pgr* morpholine (MO) and *pgr* mRNA injected embryos exposed to leflunomide in the presence and absence of progesterone. Number of embryos displaying the presented phenotype is indicated. Scale bars represent 200μm. (c) qPCR for *pgr* on zebrafish embryos at 24hpf using two different primer sets. (*pgr* primer set 1; n = 4, *pgr* primer set 2; n = 3 biologically independent experiments, Mean ± SD, Unpaired T-test with Welch Correction, * p = 0.017, ** p = 0.002, *** p = 0.021). (d) Co-Immunoprecipitation followed by mass-spectrometry of

pgr:flag:T2A:gfp injected embryos identified complex association partners of Pgr *in vivo*. (e) DDX21 associates with PGR in A375 melanoma cells (2 biologically independent experiments). Source data are available online.

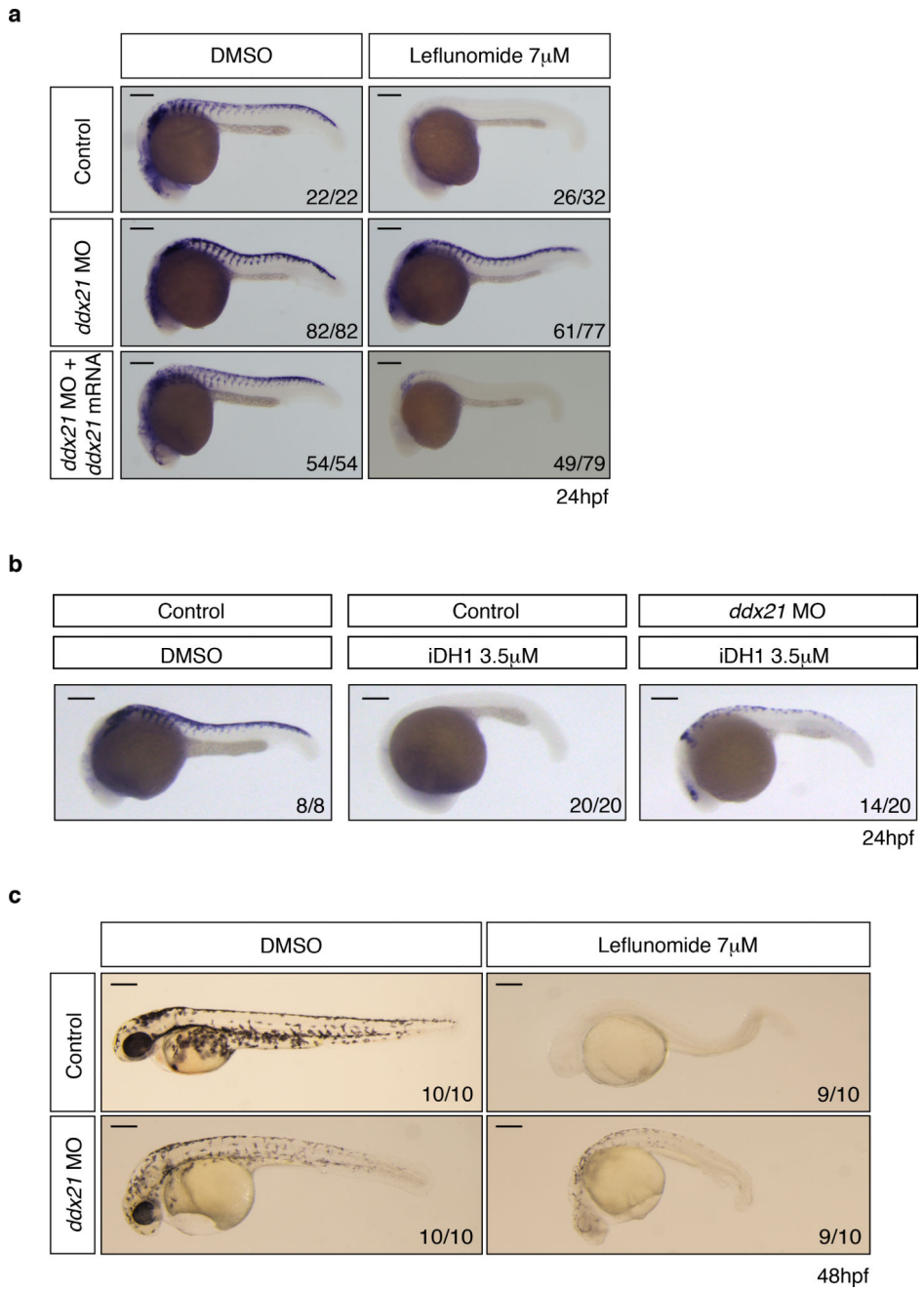

Figure 3. Loss of Ddx21 rescues neural crest defects under nucleotide depletion.

(a, b) *In situ* hybridization at 24hpf for *crestin* in control, *ddx21* morpholine (MO) and *ddx21* mRNA injected embryos exposed to DHODH inhibitors. Number of embryos displaying the presented phenotype is indicated. Scale bars represent 200μm. (c) Lateral view of pigmentation of zebrafish embryos at 48hpf. Number of embryos displaying the phenotype represented is indicated in lower right corner. Scale bars represent 250μm.

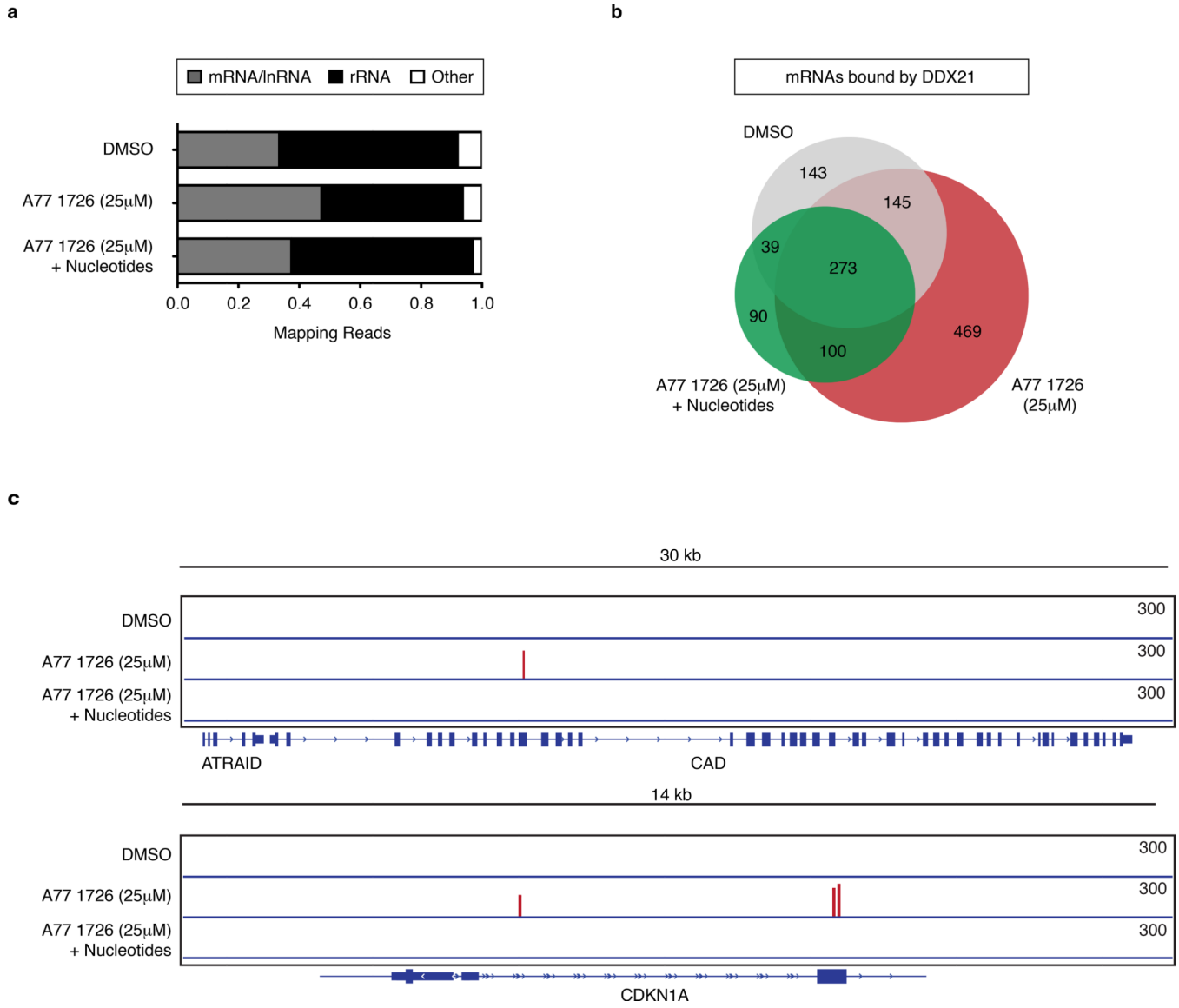

Figure 4. Nucleotide stress alters binding of DDX21 to RNA.

(a) Annotation of DDX21-associated RNAs identified by irCLIP in A375 melanoma cells after DHODH inhibition with or without nucleotide supplementation. (b) Venn diagram comparing overlap in mRNA binding targets of DDX21 under different conditions. (c) Gene tracks showing enhancer irCLIP signal of DDX21 at the CAD and CDKN1A locus during nucleotide depletion. (n = 3 biologically independent experiments). Source data are available online.

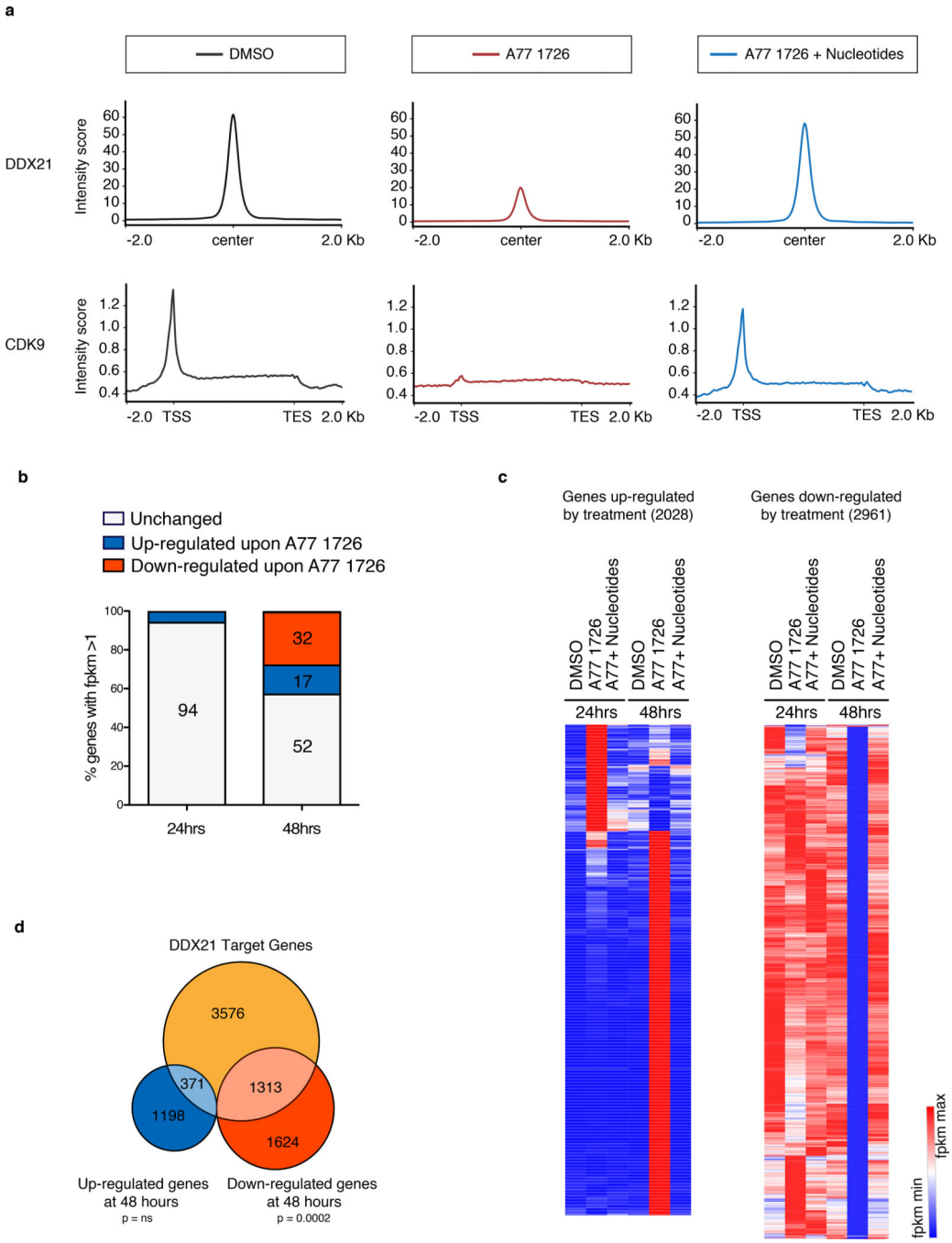

Figure 5. Ddx21 mediates transcriptional changes during nucleotide stress.

(a) ChIP-Seq for DDX21 and CDK9 in A375 melanoma cells after 24 hours of treatment. Upper panel: Metagene analysis of DDX21-bound regions. Normalized peak intensities ± 2Kb from the center of DDX21 ChIP-seq are shown. Lower panel: Metagene representation of normalized CDK9 occupancy at transcription start site (TSS), along gene bodies and at transcription end site (TES) are shown. (b) Percentage of differentially expressed genes (DEGs) in A375 melanoma cells after 24 hours and 48 hours in the presence of A77 1726. DEG criteria: FPMK ≥1 after treatment, Log2 fold change ≥1 or ≤ −1. (n = 3 biologically

independent experiments). (c) Hierarchical clustering heatmap of FPKM values from genes up-regulated (2028) and down-regulated (2961) at 24 hours and 48 hours post DHODH inhibition plus or minus nucleotide supplementation. (d) Venn diagram of DDX21 target genes with reduced DDX21 binding upon A77 1726 treatment as defined by ChIP-Seq (orange); genes up-regulated by RNA-Seq (blue) and genes down-regulated by RNA-Seq (red) at 48 hours post treatment with A77 1726 in A375 melanoma cells (n = 3 biologically independent experiments, Hypergeometric Test, ns = not significant; under enrichment p-value = 2.7e-58). Source data are available online.